A HST/COS survey of molecular hydrogen in DLAs & sub-DLAs at $z < 1$: Molecular fraction and excitation temperature

S. Muzahid[1]*, R. Srianand[2], and J. Charlton[1]

[1] *The Pennsylvania State University, 525 Davey Lab, University Park, State College, PA 16802, USA*
[2] *Inter-University Centre for Astronomy and Astrophysics, Post Bag 4, Ganeshkhind, Pune 411007, India*

ABSTRACT

We present the results of a systematic search for molecular hydrogen (H_2) in low redshift ($0.05 \lesssim z \lesssim 0.7$) DLAs and sub-DLAs with $N(\text{H\,I}) \gtrsim 10^{19.0}$ cm^{-2}, in the archival HST/COS spectra. Our core sample is comprised of 27 systems with a median $\log N(\text{H\,I}) = 19.6$. On the average, our survey is sensitive down to $\log N(H_2) = 14.4$ corresponding to a molecular fraction of $\log f_{H_2} = -4.9$ at the median $N(\text{H\,I})$. H_2 is detected in 10 cases (3/5 DLAs and 7/22 sub-DLAs) down to this f_{H_2} limit. The H_2 detection rate of 50^{+25}_{-12} percent seen in our sample, is a factor of $\gtrsim 2$ higher than that of the high-z sample of Noterdaeme et al. (2008a), for systems with $N(H_2) > 10^{14.4}$ cm^{-2}. In spite of having $N(\text{H\,I})$ values typically lower by a factor of 10, low-z H_2 systems show molecular fractions ($\log f_{H_2} = -1.93 \pm 0.63$) that are comparable to the high-z sample. The rotational excitation temperatures ($T_{01} = 133 \pm 55$ K), as measured in our low-z sample, are typically consistent with high-z measurements. Simple photoionization models favor a radiation field much weaker than the mean Galactic ISM field for a particle density in the range 10–100 cm^{-3}. The impact parameters of the identified host-galaxy candidates are in the range $10 \lesssim \rho$ (kpc) $\lesssim 80$. We, therefore, conjecture that the low-z H_2 bearing gas is not related to star-forming disks but stems from self-shielded, tidally stripped or ejected disk-material in the extended halo.

Key words: galaxies: ISM – galaxies: haloes – quasar: absorption line

1 INTRODUCTION

Damped Lyα absorbers (DLAs) and sub-DLAs seen in QSO spectra are characterized by very high neutral hydrogen column densities: $N(\text{H\,I}) \geqslant 1 \times 10^{19}$ cm^{-2} for sub-DLAs and $\geqslant 2 \times 10^{20}$ cm^{-2} for DLAs (see Wolfe et al. 2005, for a review). Whereas the ionization correction can be appreciable in sub-DLAs (Péroux et al. 2003a,b), DLAs are predominantly neutral and form the major reservoirs of neutral-gas at high redshifts (Prochaska & Wolfe 2009; Noterdaeme et al. 2009b, 2012b). In general, DLAs/sub-DLAs show higher metallicities compared to the Lyα forest systems (Schaye et al. 2003; Wolfe et al. 2005; Kulkarni et al. 2005). An increase in the cosmic mean metallicity of DLAs/sub-DLAs with cosmic time has been reported (see e.g. Prochaska et al. 2003; Kulkarni et al. 2007; Rafelski et al. 2012; Som et al. 2013). Moreover, DLA metallicities are found to be correlated with the velocity spread (Δv_{90}) of neutral or singly ionized metal lines (Wolfe & Prochaska 1998; Ledoux et al. 2006a), which has been interpreted as the mass-metallicity rela-

tion seen in galaxies (Tremonti et al. 2004). All these suggest that the DLAs/sub-DLAs are located in over-dense regions where star formation activity takes place (see e.g. Pettini et al. 1997). Direct detections of Lyα/Hα/[O III] emission lines in a handful of DLAs (Møller et al. 2004; Fynbo et al. 2010; Péroux et al. 2011; Noterdaeme et al. 2012a; Jorgenson & Wolfe 2014) made such an idea more compelling. Absorption studies of DLA/sub-DLA systems, thus, provide a unique means to probe galaxy neighbourhoods over a wide range of redshift ($0 < z < 5$) without the biases introduced in magnitude limited sample of galaxies studied in emission.

The connection between DLAs/sub-DLAs and galaxies can be firmly established by directly detecting galaxies at the same redshifts. Alternatively, such a connection can be indirectly established by showing that the physical conditions in the absorbing gas are consistent with those seen in the diffuse interstellar medium (ISM). Except the previously mentioned few cases, direct detections of candidate galaxies hosting DLAs or sub-DLAs at $z > 1.7$ have not been very successful (Kulkarni et al. 2006; Christensen et al. 2007). Thus, our understanding of the physical conditions in high-z DLAs/sub-DLAs primarily relies on the op-

* E-mail: sowgatm@gmail.com

tical absorption-line spectroscopy using low-ionization metal lines and, in a few cases, H_2, HD, and CO molecular absorption (e.g. Ledoux et al. 2003; Srianand et al. 2005, 2008; Noterdaeme et al. 2008a,b, 2009a, 2010; Tumlinson et al. 2010; Guimarães et al. 2012; Albornoz Vásquez et al. 2014). At low redshift ($z < 1$) it is relatively easy to detect candidate host-galaxies in most cases (Rao et al. 2011).

Molecular hydrogen (H_2) is the most abundant molecule in the universe which also acts as the most important molecular coolant. Formation of H_2 is expected on the surface of dust grains if the gas is cool, dense and mostly neutral (Gould & Salpeter 1963; Hollenbach & Salpeter 1971). In the case of warm and dust-free gas, H_2 can form via H^- ions (Jenkins & Peimbert 1997). Photo-dissociation of H_2 takes place in the energy range 11.1–13.6 eV via Lyman- and Warner-band absorption. Therefore, information on the kinetic and rotational excitation temperatures, the particle density, and the radiation field can be derived from good quality data when H_2 is detected. For example, at high redshift, DLA sub-components in which H_2 absorption is detected have typical kinetic temperature of $T = 153\pm78$ K and density of $n_H = 10$–200 cm^{-3} (Srianand et al. 2005). The typical inferred radiation field in the H_2 bearing components is of the order of the mean UV radiation field in the Galactic ISM. Systematic surveys at high redshift (i.e. $z > 1.7$, Ledoux et al. 2003; Noterdaeme et al. 2008a) have shown that the H_2 is detected in 10–20% of DLAs/sub-DLAs (but see Jorgenson et al. 2014). H_2 content is typically low and is found to be correlated with the metallicity and dust depletion, in those studies. The frequent detections of molecular hydrogen towards dusty and high-metallicity regions hints at its connection to star-forming regions (see also Petitjean et al. 2006).

In spite of having enormous diagnostic potential to probe physical conditions in different gas phases of galaxies in a luminosity unbiased way, molecular hydrogen has not been well studied at low-z. This is primarily because the atmospheric cutoff of light below 3000 Å makes ground-based observations of H_2 impossible for redshift $z < 1.7$. In addition, due to the unavailability of high resolution UV sensitive spectrographs in the past, detecting molecular hydrogen in absorption was not possible beyond the Galactic disk/halo (Savage et al. 1977; Gillmon et al. 2006) and the Magellanic Clouds (Tumlinson et al. 2002; Welty et al. 2012). The only known H_2 system at $z < 1.5$ (i.e. $z_{abs} = 1.15$ toward HE 0515–4414) was reported by Reimers et al. (2003) in HST/STIS data. The high throughput of HST/COS FUV gratings now gives us a window of opportunity to explore molecular hydrogen in low-z DLAs/sub-DLAs. The numerous UV absorption lines of H_2 from different rotational (J) levels are now accessible for absorbers with redshift as low as $z \sim 0.05$ in HST/COS spectra (see e.g. Crighton et al. 2013; Oliveira et al. 2014; Srianand et al. 2014). Here we present the results of our systematic search for low-z molecular hydrogen in DLAs/sub-DLAs that are detected in the medium resolution COS spectra from the HST archive.

This article is organized as follows. In Section 2 we discuss the observations and reduction of the spectra we have used to search for H_2 systems. In Section 3 we describe our search technique, final data sample, and the absorption line measurements. Detailed analysis of the sample is presented in Section 4. In Section 5 we discuss our results. The important findings are summarized in Section 6. Throughout this work we assume a flat ΛCDM cosmology with $H_0 = 70$ km s^{-1} Mpc^{-1}, $\Omega_M = 0.3$, and $\Omega_\Lambda = 0.7$. The wavelengths of H_2 transitions are taken from Bailly et al. (2010).

2   OBSERVATIONS AND DATA REDUCTION

We have searched for DLAs and sub-DLAs in nearly 400 far-ultraviolet (FUV) spectra of intermediate redshift quasars, observed with the HST/COS, that were available in the public HST archive before March, 2014. The properties of COS and its in-flight operations are discussed by Osterman et al. (2011) and Green et al. (2012). All the COS spectra were obtained using medium resolution ($R \sim 20,000$) FUV COS gratings (G130M and/or G160M). The data were retrieved from the HST archive and reduced using the CALCOS pipeline software. The pipeline reduced data (so called "$x1d$" files) were flux calibrated. To increase the spectral signal-to-noise ratio (SNR), individual G130M and G160M integrations were aligned and coadded using the IDL code ("$coadd\_x1d$") developed by Danforth et al. (2010)[1]. The exposures were weighted by the integration time while coadding in flux units. Since our data comes from different observing programs, the final data sample show a range in spectral SNR (e.g. ~ 5 to 25 per resolution element). To take care of this SNR differences, in the next section, we have defined the "H_2 sensitivity" limit for each detected DLA and sub-DLA. Depending on the spectral SNR, the "H_2 sensitivity" limit varies between $10^{13.9} - 10^{15.6}$ cm^{-2} with a median value of $10^{14.4}$ cm^{-2}. Therefore, about half of the spectra in our sample are sensitive enough to detect H_2 with $N(H_2) > 10^{14.4}$ cm^{-2}. All the low-z H_2 bearing systems show $N(H_2)$ higher than this median value.

As the COS FUV spectra are significantly oversampled (i.e. six raw pixels per resolution element), we binned the data by three pixels. This further improves SNR per pixel. All our measurements and analyses were, subsequently, performed on the binned data. Measurements are, however, found to be fairly independent of binning. Continuum normalization was done by fitting the line-free regions with a smooth lower-order polynomial.

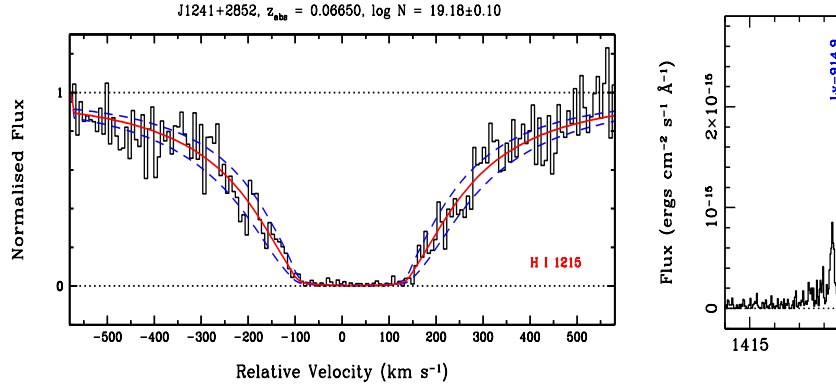## 3   SEARCH TECHNIQUE, DATA SAMPLE, AND ABSORPTION LINE MEASUREMENTS

First of all, we do not perform a blind search for H_2 systems in the spectra. Instead, we search for DLAs/sub-DLAs first and then look for H_2 absorption from the identified DLAs/sub-DLAs. Identifying DLAs/sub-DLAs is fairly straightforward in intermediate redshift QSO spectra as they produce distinct damping wings in the Lyα absorption and as there is no Lyα forest crowding at low-z (see e.g. Fig. 1). Note that, Lyα absorption will only be covered by the COS spectra for systems with $0 < z_{abs} < 0.47$, provided both G130M and G160M data are available. With the G130M data alone, Lyα can be covered up to $0 < z_{abs} \lesssim 0.19$. Therefore, in order to account for the systems for which Lyα absorption is not covered, we searched for systems that produce a strong Lyman limit ($\lambda_{rest} = 912$ Å) break and/or show strong Lyman series lines as shown in the right panel of Fig. 1. Using this conservative approach we made sure that none of the systems with $N(H_I) \gtrsim 10^{19}$ cm^{-2} are missed. In total we have found 33 systems with $\log N(H_I) \gtrsim 19.0$ as listed by increasing absorption redshift (z_{abs}) in Table 1 & 2. Our core sample, for which Lyman- and Warner-band absorption lines of H_2 are covered by the COS spectra, is comprised of the 27 systems that are listed in Table 1. In Table 2 we have listed six other systems with $\log N(H_I) \gtrsim 19.0$ for which H_2 information is not available in the existing spectra. Note

---

[1] http://casa.colorado.edu/danforth/science/cos/costools.html

Table 1. Core sample of low-z DLAs/sub-DLAs for which H$_2$ information is available.

QSO[1]	$z_{\rm em}$[2]	PID[3]	PI[4]	$z_{\rm abs}$[5]	$\log N({\rm H\,I})$[6]	$\log N({\rm H_2})$[7] Sensitivity	$\log N({\rm H_2})$[8]	$\log f_{\rm H_2}$[9]	ρ[10] (kpc)
(1)	(2)	(3)	(4)	(5)	(6)	(7)	(8)	(9)	(10)
PG1216+069	0.331	12025	J. Green	0.00635	19.32 ± 0.03^a	17.8	$<17.8^a$	$<-1.24^a$	121^a
MRK486	0.039	12276	B. Wakker	0.03879	20.25 ± 0.25	15.6	<15.6	<-4.35	
J1241+2852	0.589	12603	T. Heckman	0.06650	19.18 ± 0.10	14.9	16.45 ± 0.12	-2.43 ± 0.16	
J1553+3548	0.723	11598	J. Tumlinson	0.08300	19.55 ± 0.15^b	14.6	<14.6	<-4.65	
J1619+3342	0.472	11598	J. Tumlinson	0.09630	20.55 ± 0.10^b	14.4	18.57 ± 0.06^c	-1.69 ± 0.11^c	14^c
Q0439-433	0.594	12536	V. Kulkarni	0.10115	19.63 ± 0.08	14.2	16.64 ± 0.05	-2.69 ± 0.09	8 (Pet96)
J0928+6025	0.296	11598	J. Tumlinson	0.15380	19.35 ± 0.15^b	14.5	<14.5	<-4.55	91 (Wer13)
PHL1226	0.404	12536	V. Kulkarni	0.15962	19.37 ± 0.10	14.3	<14.3	<-4.77	
Q0850+440	0.515	13398	C. Churchill	0.16375	19.67 ± 0.10^d	13.9	15.05 ± 0.07	-4.32 ± 0.12	24 (Kac11)
B0120-28	0.434	12204	C. Thom	0.18562	20.50 ± 0.10^e	13.9	20.00 ± 0.10^e	-0.41 ± 0.12^e	70^e
J1435+3604	0.430	11598	J. Tumlinson	0.20260	19.80 ± 0.10^b	14.4	<14.4	<-5.10	39 (Wer13)
J1342-0053	0.326	11598	J. Tumlinson	0.22711	$19.0^{+0.5\,f}_{-0.8}$	14.2	14.63 ± 0.06	$-4.07^{+0.50}_{-0.80}$	35 (Wer13)
J0925+4004	0.472	11598	J. Tumlinson	0.24788	19.55 ± 0.15^b	14.6	18.82 ± 0.13	-0.57 ± 0.17	83 (Wer13)
J1001+5944	0.747	12248	J. Tumlinson	0.30350	19.32 ± 0.10^g	14.1	<14.1	<-4.92	
J1616+4154	0.441	11598	J. Tumlinson	0.32110	20.60 ± 0.20^b	14.2	19.26 ± 0.09	-1.08 ± 0.20	Not found^g
Q1323+343	0.443	12593	D. Nestor	0.35300	18.92 ± 0.20	14.5	<14.5	<-4.12	
Q1400+553	0.840	12593	D. Nestor	0.36475	20.11 ± 0.20	14.5	<14.5	<-5.31	
J0209-0438	1.132	12264	S. Morris	0.39055	19.00 ± 0.12^h	14.0	<14.0	<-4.70	
Q1232-022	1.043	12593	D. Nestor	0.39495	20.79 ± 0.20	14.8	<14.8	<-5.69	
Q1251+463	1.460	12593	D. Nestor	0.39662	20.50 ± 0.20	14.4	<14.4	<-5.80	
Q0454-2203	0.533	12466	J. Charlton	0.47437	19.97 ± 0.15^i	14.0	<14.0	<-5.67	
Q0454-2203	0.533	12466	J. Charlton	0.48321	$19.59\pm0.10^{j,k}$	14.0	<14.0	<-5.29	108 (Kac11)
J1240+0949	1.045	11698	M. Putman	0.49471	18.99 ± 0.18^j	14.5	<14.5	<-4.19	
J1236+0600	1.286	11698	M. Putman	0.54102	19.88 ± 0.46^j	15.3	<15.3	<-4.28	
Q1241+176	1.273	12466	J. Charlton	0.55048	$>19.00^l$	14.3	15.81 ± 0.17	<-2.89	21 (Kac11)
Q0107-0232	0.728	11585	N. Crighton	0.55733	19.50 ± 0.20^m	14.0	17.27 ± 0.30^m	-1.93 ± 0.36^m	10^m
Q1317+227	1.022	11667	C. Churchill	0.66047	$19.65\pm0.10^{j,n}$	14.1	<14.1	<-5.25	104 (Kac11)

Notes – [1]QSO name. [2]Emission redshift of QSO. [3]HST proposal ID. [4]Principal investigator. [5]Absorption redshift. [6]Logarithmic neutral hydrogen column density. [7]H$_2$ detection sensitivity of the spectrum at 3σ level. [8]Total H$_2$ column density when detected, else a 3σ upper limit is given. [9]Molecular mass fraction. [10]Impact parameter of the nearest possible host-galaxy candidate when available. References for ρ: Pet96–Petitjean et al. (1996); Wer13–Werk et al. (2013); Kac11–Kacprzak et al. (2011) [a]From Tripp et al. (2005), a 3σ upper limit on $N({\rm H_2})$ is obtained from FUSE spectrum. [b]From Meiring et al. (2011). [c]From Srianand et al. (2014). [d]$\log N({\rm H\,I})$ = 19.81±0.04 (Lanzetta et al. 1997, using low resolution data). [e]From Oliveira et al. (2014). [f]From Werk et al. (2014). [g]From Battisti et al. (2012). [h]$\log N({\rm H\,I})$ = 18.87±0.03 (Tejos et al. 2014). [i]$\log N({\rm H\,I})$ = $19.45^{+0.02}_{-0.03}$ (Rao et al. 2006, using low resolution data). [j]$N({\rm H\,I})$ is estimated from Voigt profile fitting of higher order Lyman series lines with minimum number of components. Therefore, $N({\rm H\,I})$ value should be taken with caution. [k]$\log N({\rm H\,I})$ = 18.65±0.02 (Rao et al. 2006, using low resolution data). [l]$N({\rm H\,I})$ is not well constrained from the COS spectrum due to blend, so we adopt a conservative lower limit; $\log N({\rm H\,I})$ = $18.90^{+0.07}_{-0.09}$ (Rao et al. 2006, using low resolution data). [m]From Crighton et al. (2013). [n]$\log N({\rm H\,I})$ = 18.57±0.02 (Rao et al. 2006, using low resolution data).
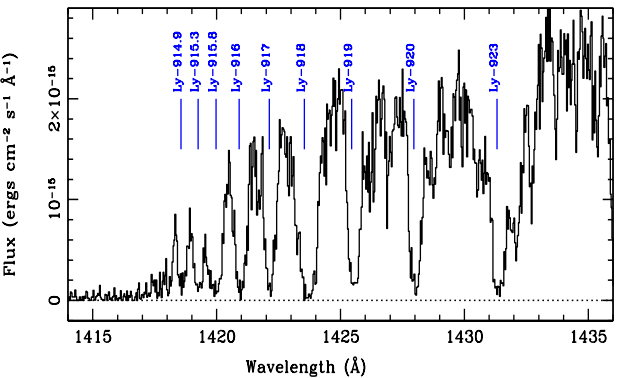

Figure 1. Left: Sub-damped Lyα absorption from the $z_{\rm abs}$ = 0.06650 towards J 1241+2852 system. The solid (red) and dashed (blue) curves represent best fitting Voigt profile to the data (black histogram) and its 1σ uncertainty, respectively. Fits for other systems are shown in Appendix-A & B. Right: Strong Lyman limit break from the $z_{\rm abs}$ = 0.55048 towards Q 1241+176 system. The Lyα is not covered in COS whereas the Lyβ falls in the gap of the existing spectrum. Both the systems show H$_2$ absorption.
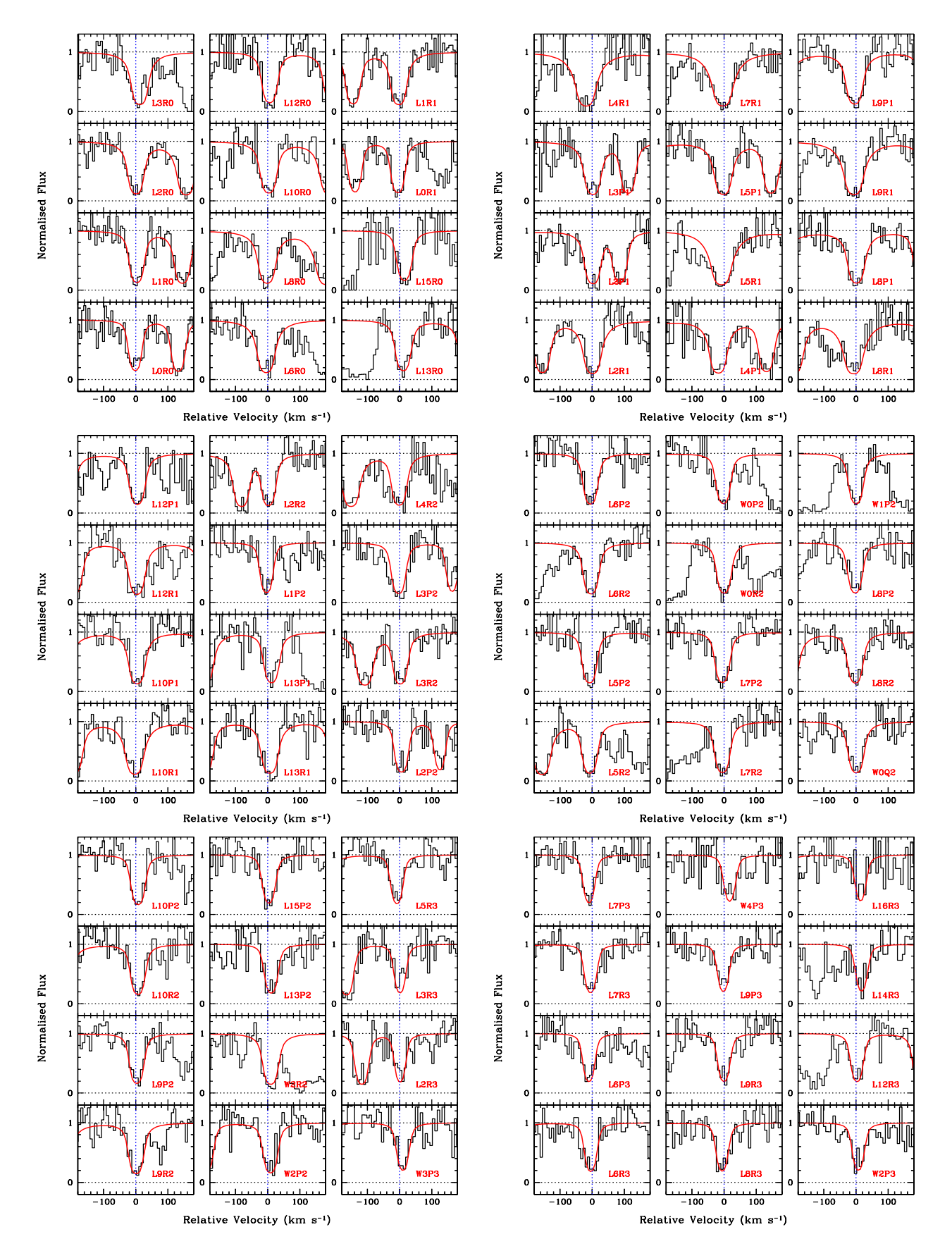
Figure 2. Numerous molecular hydrogen absorption lines from different J levels from the $z_{abs} = 0.24788$ towards J 0925+4004 system. The (red) smooth curves are the best fitting Voigt profiles to the data (in black histogram).

Table 2. Low-z DLAs/sub-DLAs for which H$_2$ information is not available.

QSO	PID	PI	z_{abs}	$\log N(\mathrm{H\,I})$
J1407+5507	12486	D. Bowen	0.00474[a]	19.75±0.05
J1415+1634	12486	D. Bowen	0.00775[a]	19.70±0.10
J0930+2848	12603	T. Heckman	0.02264[a]	20.71±0.15
J1512+0128	12603	T. Heckman	0.02948[a]	20.27±0.15
J1009+0713	11598	J. Tumlinson	0.11400[b]	20.68±0.10[d]
Q1659+373	12593	D. Nestor	0.19983[c]	19.37±0.20

Notes – [a]No H$_2$ coverage. [b]The expected wavelength range of H$_2$ transitions are covered but there is no flux below λ1241 Å due to the complete Lyman limit break from $z_{\mathrm{abs}} = 0.35590$ system. [c]Only G160M spectrum is available in which H$_2$ transitions are not covered. [d]From Meiring et al. (2011).

that for 20 of these 27 systems, $N(\mathrm{H\,I})$ are constrained from the Lyα profiles. For the other 7 systems, $N(\mathrm{H\,I})$ are constrained from Lyβ and/or higher order Lyman series lines and thus $N(\mathrm{H\,I})$ values should be taken with caution. For these systems we adopted a minimum number of components approach to fit all the unblended Lyman series lines simultaneously. Using low resolution spectra covering Lyα absorption, 5 out of the 7 systems were reported to have large $N(\mathrm{H\,I})$ values (i.e. $\log N(\mathrm{H\,I}) > 18.5$, see the footnote of Table 1). Note that for all the systems listed in Table 2, $N(\mathrm{H\,I})$ is constrained from Lyα profiles.

For every identified DLAs/sub-DLAs in Table 1, we have searched for the Lyman- and Warner-band absorption lines from the molecular hydrogen. Numerous absorption lines from different rotational levels (starting from $J = 0$) have been searched one-by-one. In total we have found 10 systems where H$_2$ absorption lines are detected. Three of these 10 systems, i.e. $z_{\mathrm{abs}} = 0.55733$ towards Q 0107–0232, (Crighton et al. 2013); $z_{\mathrm{abs}} = 0.18562$ towards B 0120–28, (Oliveira et al. 2014); and $z_{\mathrm{abs}} = 0.09630$ towards J 1619+3342, (Srianand et al. 2014) were known to have H$_2$ before. Here we report seven new H$_2$ detections.

For each of the seven cases with new H$_2$ detections, we choose a set of clean (free from severe blending) H$_2$ lines from different J levels for Voigt profile fitting. We fit all these clean lines simultaneously by keeping the Doppler-parameter (b) tied. In addition, we constrain the column density to be same for all the transitions from a given J level and allow it to be different for different J levels. The COS wavelength calibration is known to have uncertainties at the level of $10 - 15$ km s^{-1} (Savage et al. 2011; Meiring et al. 2013). Therefore, we did allow the redshift of individual transitions to be different. In majority of the cases lines are aligned within ± 5 km s^{-1}. However, occasionally, the velocity offset can be up to 20 km s^{-1}. Such extreme offsets are noticed only when the lines fall at the edge of the spectra. As an example, in Fig. 2 we show our H$_2$ fits for the $z_{\mathrm{abs}} = 0.24788$ system towards J 0925+4004. All the H$_2$ lines, from different J levels, that are used for fitting are shown in the plot. Voigt profile fits to H$_2$ absorption from all other newly reported systems are shown in Appendix-C. The line spread function (LSF) of the COS spectrograph is not a Gaussian. A characterization of the non-Gaussian LSF for COS can be found in Ghavamian et al. (2009) and Kriss (2011). For our Voigt profile fit analysis we adopt the latest LSF given by Kriss (2011). Interpolated LSFs at the line center were convolved with the model Voigt profile while fitting an absorption line using the VPFIT[2] software.

In the case of non-detections we estimate 3σ upper limits on $N(\mathrm{H}_2)$, based on the observed error in the continuum, using the fol-

lowing steps: (a) First we identify the expected wavelength ranges of H$_2$ transitions from $J = 0$ and $J = 1$ rotational levels that are uncontaminated by absorption from other systems. (b) We derive upper limits on $N(\mathrm{H}_2)$ for each of those transitions using the prescription by Hellsten et al. (1998), assuming a b-parameter of 10 km s^{-1} (close to the median $b(\mathrm{H}_2)$ in our sample) for the unresolved H$_2$ line. (c) We adopt the best limiting H$_2$ column densities we get for $J = 0$ and $J = 1$ levels. (d) Finally, we sum the $N(\mathrm{H}_2)$ limits that we get from $J = 0$ and $J = 1$ levels. The estimated upper limits are given in column 8 of Table 1. In column 7 of Table 1 we present the H$_2$ detection sensitivity, for each spectrum in our sample, at 3σ level. For the systems in which H$_2$ is not detected, the H$_2$ detection sensitivity is the same as the 3σ upper limits on $N(\mathrm{H}_2)$ presented in column 8 of Table 1. For the systems with H$_2$ detections, we estimate 3σ upper limits on $N(\mathrm{H}_2)$, as described above, from the SNR in the unabsorbed pixels near to the absorption. About half of the spectra in the core sample are sensitive down to $\log N(\mathrm{H}_2) = 14.4$, which we denote as the "median sensitivity" limit for our sample.

In Table 3 we provide H$_2$ column densities for different J levels, $N(\mathrm{H}_2, J)$, rotational excitation temperatures, T_{ij}, Doppler parameters, $b(\mathrm{H}_2)$, and average metallicities for the 10 H$_2$ bearing systems. All the newly reported H$_2$ systems, except one, are fitted with a single component Voigt profile (see column 2 of Table 3). Apart from the strongest component at 0 km s^{-1}, the $z_{\mathrm{abs}} = 0.10115$ towards Q 0439–433 system shows an additional weak, tentative component at -65 km s^{-1}. In general, the $b(\mathrm{H}_2)$ values obtained in our single component Voigt profile fit, as listed in column 8 of Table 3, are slightly higher than what is typically measured in high-z DLAs. This could indicate the presence of multiple narrow components. Indeed, in cases where we have access to high resolution optical spectra (e.g. $z_{\mathrm{abs}} = 0.10115$ system towards Q 0439–433), the Na I and Ca II absorption lines show multiple narrow components. However, from high-z H$_2$ systems studied with high resolution, it is known that all the metal components need not produce H$_2$ absorption and observed H$_2$ need not necessarily be associated with the strongest metal absorption (see e.g. Rodríguez et al. 2006). Additionally, because of the wavelength scale uncertainty and relatively lower spectral resolution of COS we do not try to fit H$_2$ lines with multiple components with b-parameters much less than the spectral resolution. This could lead to underestimation of $N(\mathrm{H}_2)$ measurements and associated errors.

4 ANALYSIS

4.1 Detection Rate

As mentioned before, there are a total of 27 systems (5 DLAs and 22 sub-DLAs) in our core sample for which the COS spectra cover the expected wavelength range of H$_2$ transitions. Ten out of these 27 systems show absorption lines from molecular hydrogen. Only three of these systems are DLAs and the remaining ones are sub-DLAs. The majority of these systems show H$_2$ absorption from $J \leqslant 3$ rotational levels. None of them show higher (i.e. $J \geqslant 4$) rotational level transitions. The $z_{\mathrm{abs}} = 0.22711$ system towards J 1342–0053 is detected via $J = 1$ level transitions alone. Furthermore, for two other systems, i.e. $z_{\mathrm{abs}} = 0.06650$ towards J 1241+2852 and $z_{\mathrm{abs}} = 0.16375$ towards Q 0850+440, we do not detect any $J = 3$ level transitions. Note that Oliveira et al. (2014) did not report any $J \geqslant 2$ transitions for the $z_{\mathrm{abs}} = 0.18495$ H$_2$ component towards B 0120–28. We have verified that $J \geqslant 2$ transitions in this component are not detected.

[2] http://www.ast.cam.ac.uk/ rfc/vpfit.html

Table 3. Voigt profile fit parameters and other measured quantities for the H_2 bearing systems.

QSO	z_{abs}	$\log N(H_2)$ (cm^{-2})					$b(H_2)$	T_{01}	T_{02}	T_{13}	$\log Z/Z_\odot$
		$J=0$	$J=1$	$J=2$	$J=3$	$J=4$	(km s^{-1})	(K)	(K)	(K)	
(1)	(2)	(3)	(4)	(5)	(6)	(7)	(8)	(9)	(10)	(11)	(12)
J1241+2852	0.06650	15.72±0.08	16.30±0.06	15.45±0.08	< 14.8[1]	< 14.7[1]	17.1±1.1	197	229	...[3]	−0.62±0.13[a]
J1619+3342[b]	0.09630	18.17±0.04	18.36±0.04	15.97±0.25	15.27±0.29	< 14.1[1]	4.1±0.4	97	77	107	−0.62±0.13[f]
Q0439-433	0.10091	14.67±0.05	15.21±0.02	14.91±0.04	14.52±0.07	< 14.1[1]	32.7±2.6	178	484	350	+0.32±0.14[a]
	0.10115	15.98±0.06	16.38±0.05	15.70±0.04	15.56±0.04	< 14.1[1]	12.0±0.5	133	227	311	
Q0850+440	0.16375	14.40±0.03	14.83±0.02	14.33±0.06	< 13.7[1]	< 13.6[1]	11.9±0.8	141	289	...[3]	< −1.36[c]
B0120-28[d]	0.18495	16.14±0.14	17.23±0.08	< 14.2[1]	< 14.5[1]	< 13.8[1]	...[2]	...[3]	...[3]	...[3]	−1.19±0.21
	0.18524	16.80±0.13	17.45±0.08	$14.55^{+0.16}_{-0.08}$	14.21±0.10	< 13.5[1]	...[2]	243	75	103	
	0.18550	$16.81^{+0.87}_{-0.22}$	18.91±0.07	18.32±0.05	17.73±0.05	< 13.9[1]	...[2]	87	...[3]	239	
	0.18568	19.72±0.02	19.53±0.03	18.40±0.04	17.60±0.05	< 13.8[1]	...[2]	65	110	161	
J1342-0053	0.22711	< 13.4[1]	14.63±0.06	< 13.6[1]	< 14.0[1]	< 14.1[1]	10.1±2.3	...[3]	...[3]	...[3]	−0.40[e]
J0925+4004	0.24788	18.15±0.08	18.63±0.04	17.90±0.10	16.83±0.15	< 14.3[1]	8.4±0.5	156	234	171	−0.29±0.17[f]
J1616+4154	0.32110	18.95±0.02	18.93±0.02	17.83±0.09	16.99±0.12	< 14.0[1]	6.9±0.5	76	122	160	−0.38±0.23[f]
Q1241+176	0.55048	15.35±0.13	15.42±0.06	14.95±0.05	14.80±0.08	< 14.0[1]	7.8±0.4	83	202	375	< +0.18[a]
Q0107-0232[g]	0.55715	16.17±0.25	17.05±0.28	16.19±0.19	15.77±0.12	< 14.0[1]	6.7±0.6	997	327	225	−0.72±0.32
	0.55729	15.63±0.39	16.42±0.40	15.65±0.25	15.47±0.18	< 14.0[1]	4.3±0.7	450	327	281	

Notes – [1]Not detected, a formal 3σ upper limit is given. [2]Not reported by (Oliveira et al. 2014). [3]Temperature is undefined. [a]Average metallicities ([S/H] or [Si/H]) from this work without ionization correction. [b]All values are taken from Srianand et al. (2014). [c]From Lanzetta et al. (1997). [d]All values are taken from Oliveira et al. (2014). [e]From Werk et al. (2013). [f]From Battisti et al. (2012). [g]All values are taken from Crighton et al. (2013) except the excitation temperatures.

At high redshift ($1.8 < z_{abs} < 4.2$) Noterdaeme et al. (2008a, hereafter N08) have conducted a survey of molecular hydrogen in DLAs and strong sub-DLAs (with $\log N(H\,I) > 20.0$) using high resolution spectra obtained with the Very Large Telescope (VLT) Ultraviolet and Visual Echelle Spectrograph (UVES). The spectral resolution ($R \sim 45,000$) and the typical SNR of their optical spectra are higher than our present survey. They have found only 13 systems with H_2 detections in a sample of 77 DLAs/sub-DLAs. Therefore, it appears that the H_2 detection is much more frequent at low-z compared to high-z. We quantify this in Fig. 3, where we have compared the H_2 detection rates in the high and low redshift samples for different $N(H_2)$ threshold values. In order to estimate detection rate for a given threshold value, we use *only* spectra that are sensitive to detect H_2 down to the threshold $N(H_2)$. The detection rate is then derived by taking the ratio of number of systems in which H_2 is detected with $N(H_2)$ higher than the threshold value to the total number of systems detected in those spectra. As mentioned before, the "median sensitivity" of our sample is $\log N(H_2) = 14.4$ whereas for the high-z sample it is $\log N(H_2) = 14.2$. Note that for the 13 high-z H_2 systems of N08 sample we have derived the spectral sensitivity for H_2 detection at 3σ level in the same fashion as described in the previous section.

It is apparent from Fig. 3 that the H_2 detection rate is higher at low-z for the whole range of $N(H_2)$ threshold values up to $\log N(H_2) = 16.5$. The difference is increasingly higher for lower $N(H_2)$ thresholds. For a threshold column density of $\log N(H_2) = 14.4$, the H_2 detection rate at low-z is 50^{+25}_{-12} percent, whereas it is only 18^{+8}_{-4} percent at high-z. Therefore, the H_2 detection rate is $\gtrsim 2$ times higher at low-z with a $\sim 2\sigma$ confidence. Recently, in a blind survey for H_2 in DLAs, observed with mostly low spectral resolution (~ 71 km s^{-1}) data, Jorgenson et al. (2014) have found a paucity of strong H_2 systems (e.g. ~ 1 percent detection rate for $\log N(H_2) > 18$). For a $N(H_2)$ threshold as high as 10^{18} cm^{-2}, the H_2 detection rate in our low-z sample (i.e. 15^{+12}_{-4} percent) is higher than that found by Jorgenson et al. (2014) but consistent with the sample of N08 (i.e. 10^{+5}_{-3} percent). In passing, we wish to point out that using high redshift ($z > 2$) QSO spectra from the Sloan Digital Sky Survey (SDSS), Balashev et al. (2014) have
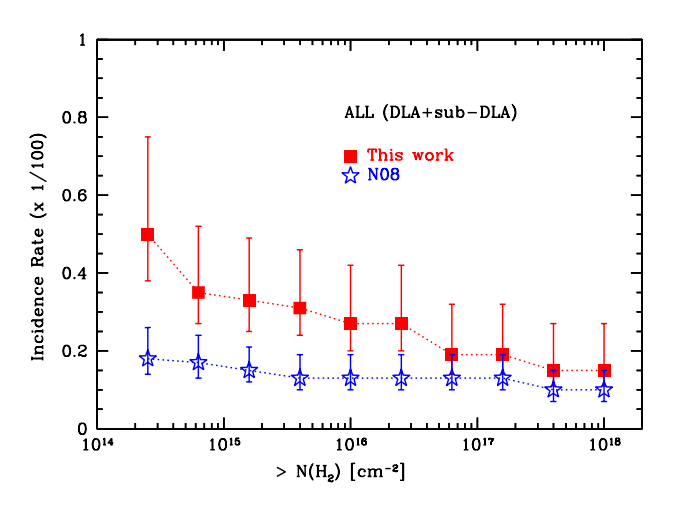

Figure 3. Detection rates of molecular hydrogen for our low-z sample (red squares) and the high-z sample of N08 (blue stars) against different threshold $N(H_2)$ values. Errorbars represent Gaussian 1σ confidence intervals computed using tables of Gehrels (1986) assuming a Poisson distribution.

found an upper limit in detection rate of ~ 7 percent for strong H_2 systems with $\log N(H_2) > 19.0$. For our sample, we find a detection rate of 7^{+10}_{-2} percent for a similar $N(H_2)$ threshold.

4.2 Column density distributions

The total H_2 column density of a given system with detected H_2, as listed in column 8 of Table 1, is derived by summing the column densities measured in different J levels as listed in columns 3, 4, 5, and 6 of Table 3. For multicomponent systems, component column densities are further summed up to get the total $N(H_2)$. The total H_2 column density distribution for our low-z sample is compared with that of the high-z sample of N08 in the left panel of Fig. 4. We do not find any significant difference between them. A two-sided Kolmogorov-Smirnov (KS) test suggests that the maxi-
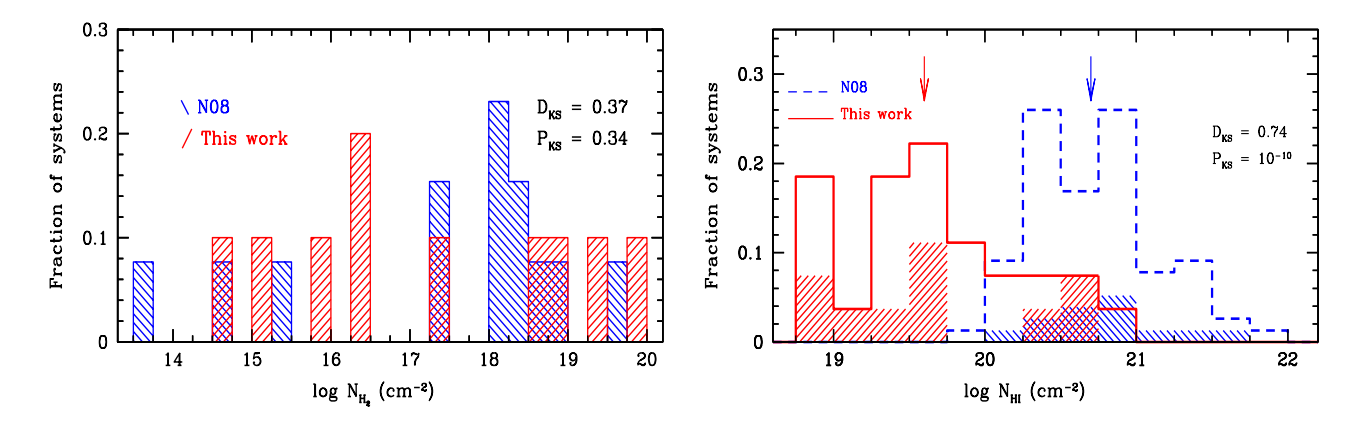
Figure 4. Left: The $N(H_2)$ distributions for the low-z sample (red 45° hatched histogram) and the high-z sample of N08 (blue 135° hatched histogram). Right: The $N(H\,\textsc{i})$ distributions of our core sample (red solid histogram) and the sample of N08 (blue dashed histogram). The arrows mark the median values. The (red) 45° and (blue) 135° hatched histograms show the $N(H\,\textsc{i})$ distributions for the systems with H_2 detections in low- and high-z samples respectively.

mum deviation between the two cumulative distribution functions is $D_{KS} = 0.37$ with a probability of $P_{KS} = 0.34$[3].

In the right panel of Fig. 4 the H I column density distributions of our core sample (total 27 systems) and the sample of N08 (total 77 systems) are shown. It is clearly evident that the two distributions are significantly different. A two-sided KS-test also supports this with a $D_{KS} = 0.74$ and a $P_{KS} \sim 10^{-10}$. The median value of $\log N(H\,\textsc{i}) = 19.6$ for our low-z sample is an order of magnitude lower than that of the high-z sample. In the low-z sample only 7 systems show $\log N(H\,\textsc{i}) > 20.0$, whereas all 77 high-$z$ systems have $\log N(H\,\textsc{i}) > 20.0$. Therefore, in order to make a more realistic comparison between properties of H_2 absorbers at high- and low-z, it is important to increase the sample sizes of the sub-DLAs at high-z and the DLAs at low-z.

The hatched histograms in the right panel of Fig. 4 show the $N(H\,\textsc{i})$ distributions for the systems in which H_2 is detected. It is interesting to note that there is no preference for molecular hydrogen to originate from higher (or lower) $N(H\,\textsc{i})$ systems. A two-sided KS-test suggests that the $N(H\,\textsc{i})$ distributions for systems with and without H_2 detections are very similar (e.g. $D_{KS} = 0.18$ and $P_{KS} = 0.97$). Moreover, we do not find any significant correlation between $N(H\,\textsc{i})$ and $N(H_2)$. N08 have found the same for their high-z sample. As noted earlier, a significant fraction (i.e. 7 out of 10) of low-z H_2 systems show $\log N(H\,\textsc{i}) < 20$. Detection of H_2 at lower $N(H\,\textsc{i})$ and the enhanced detection rate could possibly suggest that the low-z sub-DLAs have (a) higher metallicities and/or dust, (b) higher densities, and/or (c) weaker radiation field. We discuss these issues in Section 5.

4.3 The molecular fraction, f_{H_2}

The molecular fraction, f_{H_2}, of a DLA/sub-DLA system is defined as:

$$f_{H_2} = \frac{2N(H_2)}{N(H\,\textsc{i}) + 2N(H_2)}. \qquad (1)$$

At the median $N(H\,\textsc{i})$, the "median sensitivity" limit of our survey (i.e. $\log N(H_2) = 14.4$) corresponds to a $f_{H_2} = 10^{-4.9}$. We, therefore, denote this as our median f_{H_2} sensitivity limit. In four differ-

Table 4. Results of log-rank tests between f_{H_2} distributions.

Sample-1	Sample-2	$> \log f_{H_2}^a$	$\chi^{2\,b}$	$P_{\log-\mathrm{rank}}^c$
Low-z	High-z	-8.0	6.2	0.013
Low-z	High-z	-4.9	0.6	0.444
Low-z	ISM (Halo)	-4.9	6.7	0.009
Low-z	ISM (Disk)	-4.9	14.8	10^{-4}
Low-z	SMC	-4.9	15.2	10^{-4}
Low-z	LMC	-4.9	15.2	10^{-4}

Notes – ^{a}Threshold $\log f_{H_2}$. ^{b}The χ^2 statistic for a test of equality. ^{c}Probability of rejecting null hypothesis by chance.

ent panels of Fig. 5 we have plotted f_{H_2} against total hydrogen column density, $N_H = N(H\,\textsc{i})+2N(H_2)$. We note that for sub-DLAs this is a lower limit in N_H as we are ignoring the ionized fraction.

In panel-(A) we have compared low- and high-z samples in the $f_{H_2} - N_H$ plane. As already noted, the low-z systems have lower N_H values (always $N_H < 10^{20.7} \mathrm{cm}^{-2}$) compared to high-$z$. There are a few detections with very low molecular fractions ($f_{H_2} \lesssim 10^{-4.9}$) in the high-$z$ sample. Such low f_{H_2} systems are not present in our sample. We perform a two-sample survival analysis, including censored data points (upper limits), in order to investigate if f_{H_2} distributions at high-z and low-z are drawn from the same parent populations[4]. The log-rank test rejects the null hypothesis with a confidence of 98.7% (see Table 4), suggesting only a mild difference. When we consider only systems with $\log f_{H_2} > -4.9$, the log-rank test rejects the null hypothesis with a confidence of only 56%, implying a lack of any statistically significant difference in the f_{H_2} distribution. We point out that the mild difference suggested by the log-rank test for the entire sample is merely due to the fact that the H_2 detection rate is considerably higher at low-z than at high-z.

In panel-(B) of Fig. 5 we compare our sample with that of the Savage et al. (1977, i.e. the Galactic disk) and Gillmon et al. (2006, i.e. the Galactic halo) samples. The Galactic samples clearly show a transition near $\log N_H = 20.7$, above which all systems have molecular fraction $\log f_{H_2} \gtrsim -1$. This transition, leading to a bimodality in the f_{H_2} distribution, is generally identified as

---

[3] P_{KS} is the probability of finding this D_{KS} value or lower by chance.

[4] We have used the "*survdiff*" function under the "*survival*" package in R (http://www.r-project.org/).
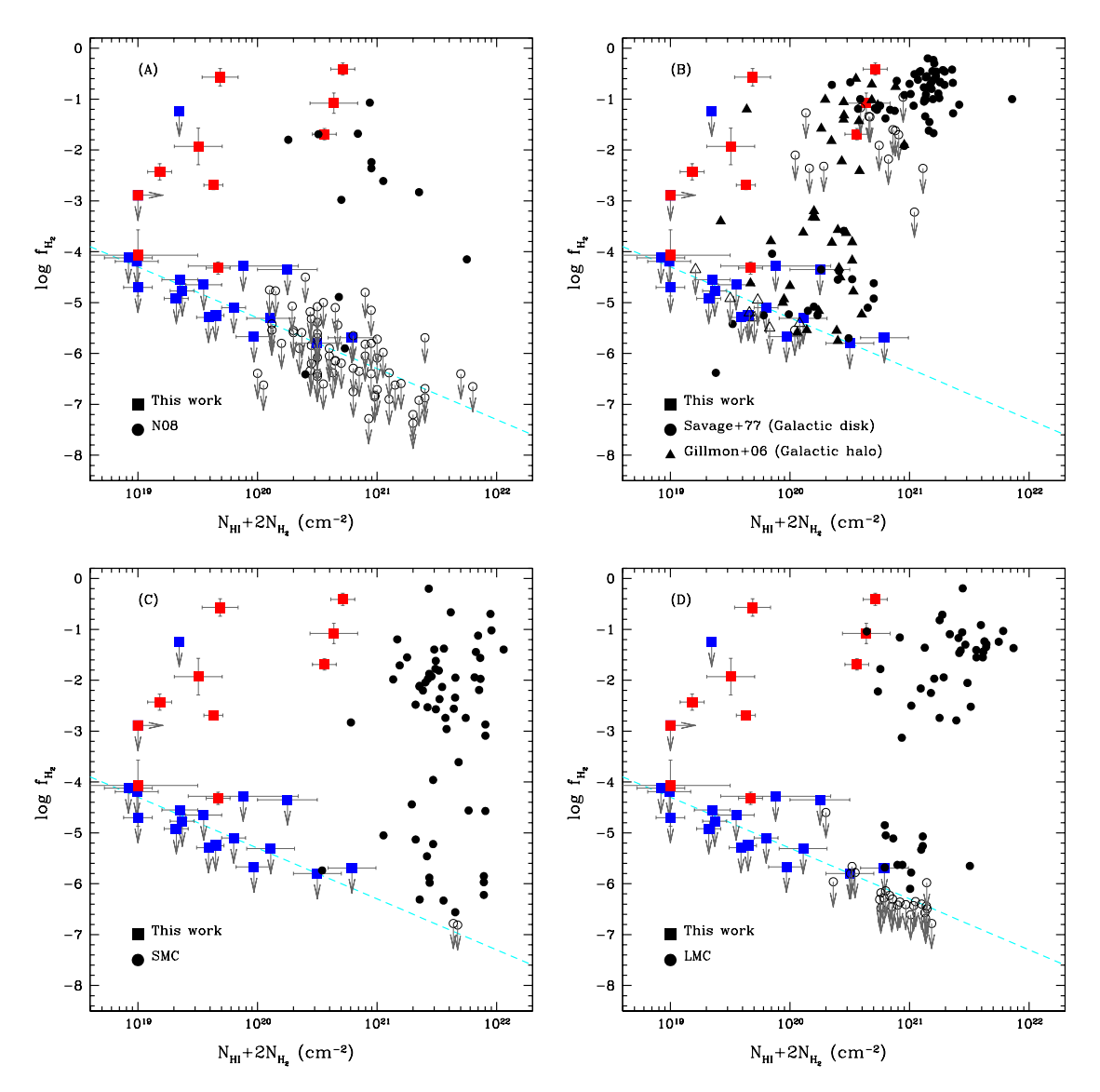
Figure 5. The molecular fraction against the total hydrogen (neutral atomic + molecular) column density, $N(\text{H\,I} + \text{H}_2)$. In each panel squares represent our low-z sample (with red squares corresponding to H_2 detections), whereas circles/triangles represent other samples as indicated in the panel (with filled ones corresponding to H_2 detections). The dashed line corresponds to our "median sensitivity" limit i.e. $\log N(\text{H}_2) = 14.4$.

the threshold above which the H_2 molecule gets completely self-shielded from interstellar radiation (Savage et al. 1977). Such a transition is not apparent in the low-z and/or high-z DLA/sub-DLA sample. This is what is expected since they trace a wide variety of environments (e.g. different metallicities, dust depletion, radiation field etc.) unlike the sightlines passing through a single galaxy. A log-rank test of the f_{H_2} distributions between our low-z sample and the Galactic disk sample of Savage et al. (1977), for systems with $\log f_{\text{H}_2} > -4.9$, indicates that they are significantly different (e.g. rejects the null-hypothesis with a confidence of $> 99.99\%$). This is also true when we compare low-z f_{H_2} distribution with that of the Galactic halo (Gillmon et al. 2006) sample, albeit with lower confidence (e.g. 99.1% confidence, see Table 4).

In panel-(C) and (D) of Fig. 5, the low-z sample is compared with the SMC and LMC, respectively. Here we have taken both Tumlinson et al. (2002) and Welty et al. (2012) measurements into account. For lines of sight that are common in both the studies,

we used updated measurements from Welty et al. (2012). It is clear that our low-z sample and the Magellanic Cloud systems have only marginal overlap, with the latter having systematically higher N_{H} values. Unlike the Galactic lines of sight, the transition in f_{H_2} due to self-shielding is not very prominent for SMC systems. LMC systems, however, show such transition albeit at higher N_{H} values (i.e. at $\log N_{\text{H}} = 21.3$). A log-rank test of f_{H_2} distributions between our low-z sample and the SMC/LMC, for systems with $\log f_{\text{H}_2} > -4.9$, suggests that they are drawn from significantly different parent populations (e.g. rejects the null-hypothesis with a probability of $> 99.99\%$, see Table 4).

It is clearly evident from Fig. 5 that our low-z H_2 systems predominantly populate the upper-left corner of the $f_{\text{H}_2} - N_{\text{H}}$ plane (i.e. $f_{\text{H}_2} \gtrsim -4.5$ and $\log N_{\text{H}} \lesssim 20.7$). This is a unique region in the parameter-space. Only one of the Magellanic Cloud systems, three high-z systems and a few (8/72) Galactic disk systems, with detected H_2, fall in this region. The key reason for this ob-

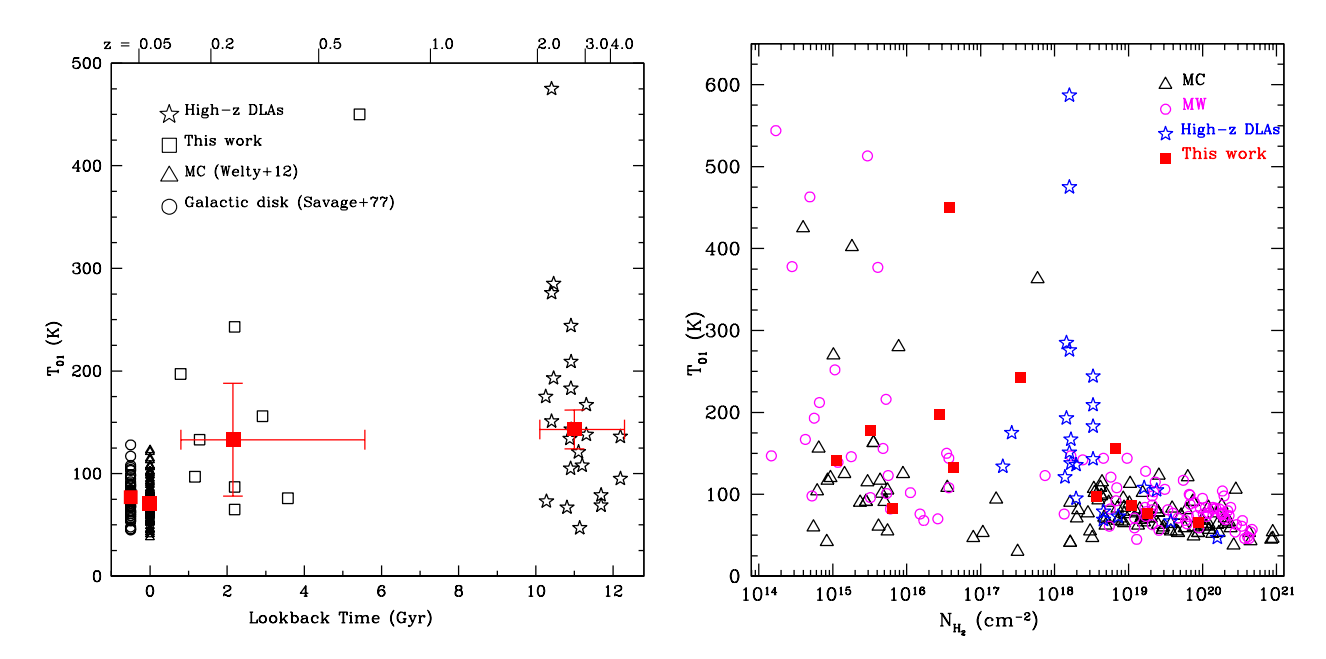**Figure 6.** Left: Cosmic evolution of the rotational excitation temperature, T_{01}. Only components with total $\log N(H_2) > 16.5$ are used. The (red) filled squares represent the median values in each sample. Error-bars along y-axis are the 1σ Gaussian errors on the median value computed from bootstrapping. Error-bars along x-axis are just to show the spread in look-back time for high- and low-z samples. The Galactic measurements are shifted to the left for clarity. Here we have excluded the temperature measurements in the $z_{abs} = 0.55715$ component towards Q 0107$-$0232. Right: T_{01} against H$_2$ column density for different samples plotted with different symbols. The (magenta) open circles (Milky Way, MW) are from Savage et al. (1977) and Gillmon et al. (2006). The (black) open triangles (Magellanic Clouds, MC) are from Tumlinson et al. (2002) and Welty et al. (2012). The (blue) stars are from the "high-z DLAs" as defined in the text. The data points plotted as (red) squares are from this study.

servation is that our low-z sample is primarily comprised of sub-DLAs. The only possible exception is the Galactic halo sample. We would like to emphasize here that a significantly large fraction (e.g. $25/40 \sim 63\%$) of the Galactic halo systems, in which H$_2$ is detected, have f_{H_2} and N_H in the range similar to as seen for our low-z sample. This perhaps indicates that the origin(s) and the physical conditions of molecular gas in low-z DLAs/sub-DLAs are similar to that of the Milky Way halo gas.

It is interesting to note that even with systematically lower N_H values, many low-z systems show a considerably large molecular fraction. We discuss possible reasons for that in view of simple photoionization models in Section 5.3. The Galactic disk/Magellanic Clouds/high-z samples are primarily composed of DLAs with $N_H > 10^{21}$ cm^{-2}. Therefore, we point out that for a realistic comparison of f_{H_2} distributions, as presented in Table 4, more observations of molecular hydrogen in DLAs at low-z are extremely important. Additionally, more observations of H$_2$ in sub-DLAs at high-z are crucial for comparing with our current low-z sample.

4.4 The excitation temperature, T_{01}

The rotational excitation temperature, T_{01}, for $J = 0$ to $J = 1$ rotational levels can be expressed as:

$$\frac{N(J=1)}{N(J=0)} = \frac{g_1}{g_0} \exp(-170.5/T_{01}) . \qquad (2)$$

Here g_0, g_1 are the statistical weights for $J = 0$ and $J = 1$ rotational levels respectively. When H$_2$ is sufficiently self-shielded (e.g. $\log N(H_2) > 16.5$) from photo-dissociating photons, collisional processes dominate the level populations, then T_{01} represents the kinetic temperature of the absorbing gas (Snow et al.

2000; Roy et al. 2006). The excitation temperatures (T_{01}) measured from H$_2$ absorption in our sample are summarized in column 9 of Table 3. The median value of T_{01} in our sample is $T_{01} = 133\pm75$ K for the H$_2$ components with a total $N(H_2) > 10^{16.5}$ cm^{-2}. The large scatter results from the large T_{01} value (i.e. 997 K) measured in one of the components in $z_{abs} = 0.55733$ towards Q 0107$-$0232 system. The median value becomes $T_{01} = 133\pm55$ K when we exclude the outlier. Note that the errors in the median T_{01} values in this work are estimated from bootstrapping unless specified.

In the left panel of Fig. 6 we show the evolution of T_{01} over the last 12 Gyr of cosmic time. Measurements from different samples at different cosmic time (or redshift) are shown in different symbols. The local measurements are taken from Savage et al. (1977, the Galactic disk) and Welty et al. (2012, the Magellanic Clouds), whereas the high-z measurements are from Petitjean et al. (2002), Srianand et al. (2005, 2008), Ledoux et al. (2006b), Noterdaeme et al. (2007, 2008a, 2010), and Guimarães et al. (2012). Hereafter, we will refer this ensemble of systems as "high-z DLAs". The median T_{01} in our low-z sample (i.e. 133 ± 55 K) is very similar to that of the "high-z DLAs" (i.e. 143 ± 19 K). The local measurements of T_{01}, i.e. 77 ± 02 K in the Galactic disk, 115 ± 13 K in the Galactic halo, and 71 ± 03 K in the Magellanic Clouds, are slightly lower but roughly consistent with the low-z measurements within the large scatter.

In the right panel of Fig. 6, T_{01} is plotted against the H$_2$ column density for various different samples. T_{01}, in general, seem to show a large scatter for lower values of $N(H_2)$. On the contrary, for $\log N(H_2) > 19.0$ all systems show $T_{01} < 120$ K, irrespective of which samples they come from. This can be understood in terms of efficient shielding of radiation in higher $N(H_2)$ systems. In columns 10 and 11 of Table 3 we present T_{02} and T_{13}, respec-
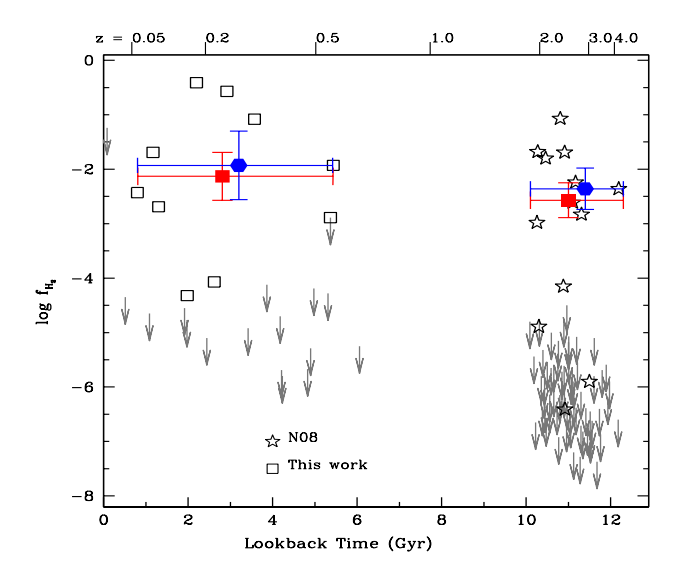
Figure 7. Cosmic evolution of the molecular fraction in DLAs/sub-DLAs. Open squares and stars represent measurements from our low-z and the high-z sample of N08, respectively. Filled (red) squares and (blue) diamonds, respectively, represent the mean and median of $\log f_{H_2}$, for the systems in which H_2 is detected with a $\log f_{H_2} > -4.9$ in each sample. The error-bars in mean and median $\log f_{H_2}$ are computed from bootstrapping. The error-bars along x-axis are just to show the spread in look-back time for each sample.

tively, estimated using Eqn. 3 of Srianand et al. (2005). These values are typically higher than the corresponding T_{01} measurements. Such elevated T_{02} and/or T_{13} values compared to T_{01} have been interpreted as the influence of radiation pumping and/or formation pumping (Tumlinson et al. 2002; Srianand et al. 2005). Higher rotational level (i.e. $J \geqslant 4$) populations (e.g. N_4/N_2 or N_5/N_3 ratios) are even more sensitive probes of radiation/formation pumping (see e.g. Tumlinson et al. 2002). None of the low-z H_2 systems show detectable absorption from $J \geqslant 4$ levels. This clearly suggests that the radiation/formation pumping is not important for the H_2 systems in our sample.

5 DISCUSSIONS

5.1 Evolution of f_{H_2}

In equilibrium between formation and photo-dissociation, the molecular fraction can be written as:

$$f_{H_2} = \frac{2Rn_{HI}}{D} , \qquad (3)$$

where, R (in cm^3 s^{-1}) is the formation rate coefficient and D (in s^{-1}) is the photo-dissociation rate. In a cold and neutral gas phase, H_2 formation occurs on the surface of dust grains. Thus, R is proportional to the dust-to-gas ratio (κ). Note that κ depends on the metallicity of the gas. The dissociation rate, D, on the other hand, depends crucially on the ionizing radiation. There are several indications that f_{H_2} should increase with cosmic time:

(a) The global star-formation rate density (or luminosity density) of galaxies decreases with time (see e.g. Bouwens et al. 2011). This suggests that if H_2 systems are related to star forming disks at all epochs, then low-z systems will experience a much weaker ionizing radiation field compared to high-z systems. This will lead to a

decrease in the photo-dissociation rate.

(b) The extra-galactic UV background radiation gets fainter by about an order of magnitude at low-z compared to high-z ($z > 2$) as a consequence of the decrease in the global star-formation rate density (Haardt & Madau 1996, 2012). This implies that if H_2 systems are related to halo gas, where extra-galactic UV background radiation dominates over the radiation field of the host-galaxy, then again low-z systems will experience a much weaker ionizing radiation compared to high-z systems.

(c) An increase in the cosmic mean metallicity of DLAs with time (Prochaska et al. 2003; Rafelski et al. 2012), suggests that the H_2 formation rate will be higher at low-z, leading to an increase in f_{H_2}. Furthermore, we note that sub-DLAs tend to show higher metallicities and faster metallicity evolution compared to DLAs (Kulkarni et al. 2007; Som et al. 2013). Nevertheless, we find that the median metallicity of our H_2 systems (listed in column 12 of Table 3) is only 0.4 dex higher than that of the N08 sample.

In Fig. 7 we show the evolution of f_{H_2} over the last 12 Gyr of cosmic time. The high- and low-z samples are presented in open stars and open squares, respectively. Upper limits in both the samples are shown by arrows. The mean and median values of $\log f_{H_2}$, for the low-z systems in which H_2 is detected with a $\log f_{H_2} > -4.9$, are found to be -2.13 ± 0.44 and -1.93 ± 0.63, respectively. These values are only ~ 2.7 times higher than the corresponding values at high-z. This could result from the fact that the $N(H_2)$ distributions at high- and low-z are very similar whereas the low-z systems have systematically lower $N(H\,I)$ values. Nevertheless, the mean/median values of $\log f_{H_2}$ at high- and low-z are consistent within 1σ allowed range. Finally, we recall from Section 3 that the $N(H_2)$ we derive from COS data could be a lower limit if the lines are narrow and unresolved or partially covering the background continuum source.

Next, we have performed the Kendall's τ correlation test including censored data points between absorption redshift and $\log f_{H_2}$[5]. No significant correlation is found when we consider only system with $\log f_{H_2} > -4.9$. However, a mild anti-correlation is suggested by the Kendall's τ test with a $\tau = -0.27$ and with a confidence of 99.99 percent, when we consider all the systems from both the high- and the low-z samples. This mild anti-correlation is essentially the manifestation of the fact that the detection rate of H_2 is considerably higher at low-z.

5.2 Enhanced detection rate of H_2 at low-z

We find that the detection rate of H_2 absorption in our low-z sample is generally higher compared to the high-z sample of N08 for different $N(H_2)$ threshold values up to $\log N(H_2) = 16.5$. In our sample the H_2 detection rate is found to be 50^{+25}_{-12} percent, for systems with $\log N(H_2) > 14.4$, detected in spectra that are sensitive down to $\log N(H_2) = 14.4$. The detection rate is a factor of $\gtrsim 2$ higher compared to the high-z sample of N08, in which it is only 18^{+8}_{-4} percent for a similar $N(H_2)$ threshold. The occurrence of enhanced H_2 detection rate at low-z is unlikely due to sample bias as none of these spectra were obtained in order to study molecular hydrogen. We note that the program ID 12593 (PI: D. Nestor) was proposed to observe low-z DLAs but no H_2 is detected from that dataset. In addition, program ID 12536 (PI: V. Kulkarni) was proposed to observe low-z sub-DLAs and one of these shows H_2

---

[5] We have used the "*cenken*" function under the "*NADA*" package in R
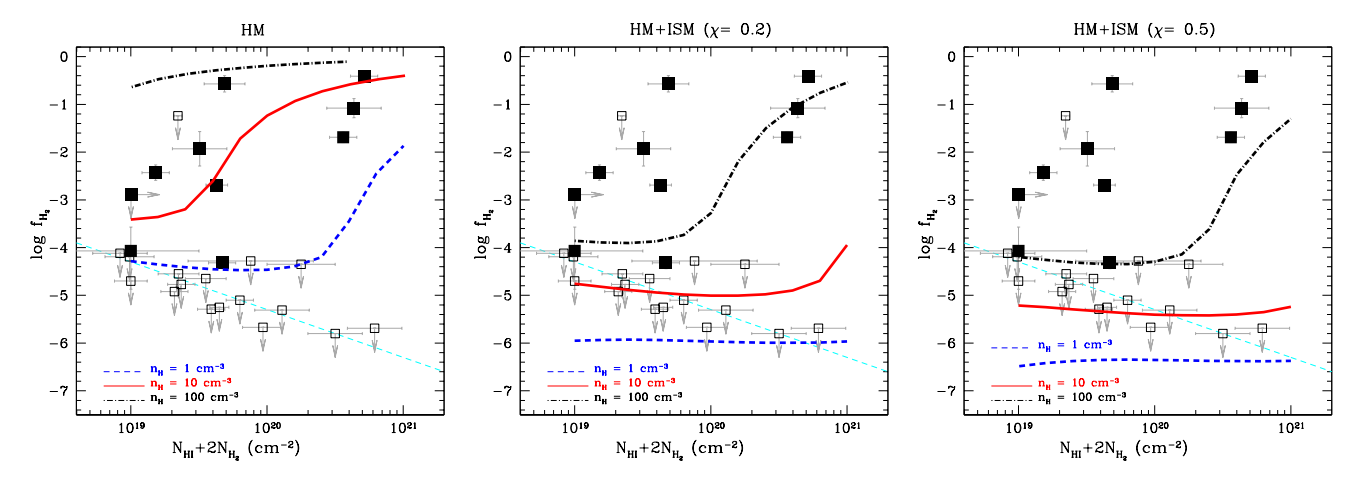
Figure 8. The molecular fraction against the total hydrogen (atomic+molecular) column density in our sample. The systems in which H$_2$ is detected are plotted as solid squares. The dashed straight line corresponds to a $\log N(H_2) = 14.4$. Results of photoionization model predictions for three representative densities are shown by smooth curves in each panel. Models of three different panels assume three different ionizing radiation (see text). All models assume a metallicity of $\log Z/Z_\odot = -0.4$ and a dust-to-gas ratio of $\log \kappa = -1.0$.

absorption. But none of these proposals were focussed on H$_2$ that was known beforehand.

As discussed in the previous section, conditions are more favorable for a molecular gas phase at low-z since the ambient radiation field intensity decreases with cosmic time. In fact, in two systems for which we have conducted detailed ionization modelling we infer a weak radiation field (see e.g. Srianand et al. 2014, and Dutta et al. (submitted)). Besides, the cosmic mean metallicity of DLAs is known to increase with cosmic time (Prochaska et al. 2003; Rafelski et al. 2012). From their best fitting metallicity versus redshift relationship, we expect the metallicity of the low-z DLAs (at $z \lesssim 0.5$) to have ~ 0.5 dex higher metallicity compared to the DLAs in the sample of N08. Moreover, sub-DLAs have higher metallicities than DLAs at any given epoch and show faster metallicity evolution (e.g. Kulkarni et al. 2007; Som et al. 2013). From Fig. 11 of Som et al. (2013) we notice that in the case of sub-DLAs at $z \lesssim 0.5$, the enhancement in the $N(\text{H\,\textsc{i}})$-weighted mean metallicity could be as high as 0.7 dex compared to sub-DLAs at $z \simeq 2.5$. Both the above mentioned facts suggest that the probability of finding a metal-rich DLA and/or sub-DLA at low-z should be higher than that at high-z. Note that the vast majority (22/27) of our low-z systems are sub-DLAs and likely to be metal rich. It has been demonstrated that metal-rich DLAs/sub-DLAs are more likely to have molecules (see e.g. Petitjean et al. 2006; Noterdaeme et al. 2008a). Thus a combination of enhanced metallicity and reduced radiation field could possibly explain the higher detection rate of molecular hydrogen at low redshift. We plan to investigate this issue in detail in our future work. In passing, we note that (i) $N(\text{H\,\textsc{i}})$ and $N(\text{H}_2)$ do not show any significant correlation and (ii) the $N(\text{H\,\textsc{i}})$ distributions for systems with and without detected H$_2$ are not significantly different. Therefore, the observed difference in the H$_2$ detection rate is not possibly due to the difference in the $N(\text{H\,\textsc{i}})$ distribution between high- and low-z samples.

5.3 Overall physical conditions

To understand the overall physical conditions in these low-z H$_2$ systems we run grids of photoionization models using CLOUDY (v13.03, last described by Ferland et al. 2013). The models predicted molecular fractions as a function of total hydrogen column

density (atomic+molecular) are shown in three different panels of Fig. 8. In each panel, models are run for three different densities (i.e. $n_\text{H} = 1$, 10, and 100 cm^{-3}), assuming a metallicity of $\log Z = -0.4$ (the median value for our sample, see column 12 of Table 3) and a dust-to-gas ratio of $\log \kappa = -1.0$ (a fiducial value). The ionizing radiation field for the models shown in the left panel is the extra-galactic UV background radiation computed by Haardt & Madau (2001) at $z = 0.2$. It is apparent from this panel that the model with $n_\text{H} = 1$ cm^{-3} cannot explain the majority of the systems where H$_2$ is detected. The model with $n_\text{H} = 10$ cm^{-3} seems to be a better choice. Now when we add the mean UV radiation field as seen in the Galactic ISM (Black 1987) but scaled by a factor of $\chi = 0.2$, the model with $n_\text{H} = 10$ cm^{-3} clearly does not work (see middle panel). A particle density of $n_\text{H} = 100$ cm^{-3} is preferred instead. If we further increase the contribution of the mean Galactic radiation field by increasing the scaling factor to a $\chi = 0.5$, even the model with $n_\text{H} = 100$ cm^{-3} fails to reproduce the observed molecular fractions (see right panel).

At high redshift, the density of the H$_2$ bearing components in DLAs found to be in the range 10–200 cm^{-3} with a radiation field of the order of or slightly higher than the mean UV radiation field in the Galactic ISM (i.e. $\chi \gtrsim 1.0$, see Srianand et al. 2005). We note that the density of the low-z H$_2$ absorbers cannot be much higher than what is seen in the diffuse atomic phase of the ISM (i.e. 10 - 100 cm^{-3}), as we do not see HD/CO molecules or the excited fine structure lines of C\,\textsc{i}/C\,\textsc{ii} from most of these systems. Weak HD absorption is detected only in one case (see Oliveira et al. 2014). If the low-z H$_2$ systems originate from a density range $10 - 100$ cm^{-3} then the UV radiation field prevailing in these systems has to be much weaker compared to the Galactic mean field (i.e. $\chi \lesssim 0.5$) and/or the inferred radiation field in high-z DLAs with detected H$_2$. Therefore, we speculate that the low-z H$_2$ systems are possibly not related to star-forming disks, but trace regions that are farther away from the luminous part of a galaxy. The large impact parameters of host-galaxy candidates, as discussed below, further promote such an idea.
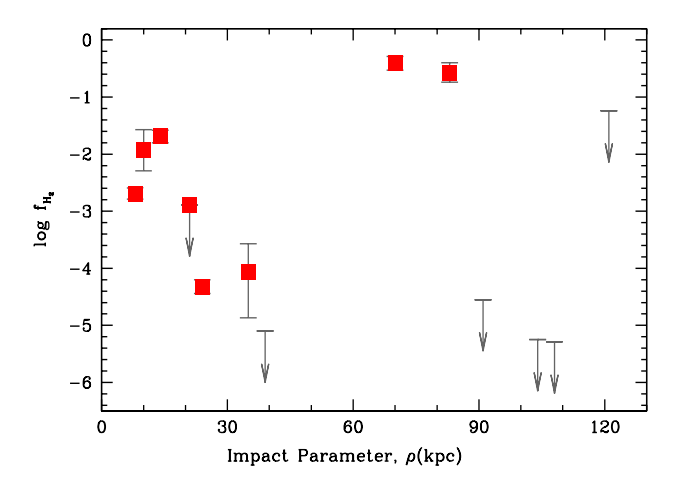
Figure 9. The molecular fractions against the host-galaxy impact parameters (see column 10 of Table 1). The arrows without squares represent systems where H_2 is not detected.

5.4 Connection to galaxies

For eight out of the ten low-z H_2 systems, we have host-galaxy information from the literature (see column 10 of Table 1). When multiple possible host-galaxy candidates are reported for a given system, the true host is considered to be the galaxy with the lowest impact parameter. In Fig. 9 we show the molecular fractions against the impact parameters of the nearest possible host-galaxy candidate for these systems. There are five more systems where H_2 absorption is not detected but the impact parameters of the nearest possible host-galaxy candidates are available. These are shown just by arrows in the figure. Note that all these five systems have $\rho > 30$ kpc. In this limited sample, there is no obvious correlation between the f_{H_2} and the impact parameter. However, the H_2 detection rate seems to be higher when the impact parameter is $\rho < 30$ kpc.

We notice that three (five) of the eight H_2 systems show $\rho < 20$ kpc (30 kpc). These are roughly consistent with the median values of impact parameters for the DLA/sub-DLA host-galaxies found by Rao et al. (2011). Nonetheless, the presence of diffuse molecular gas at impact parameters of > 15 kpc is intriguing. We therefore put forward a scenario where molecular hydrogen detected in DLAs/sub-DLAs is not related to star-forming disks but stems from halo gas. However, the density range of halo gas as suggested by the low ionization metal lines (e.g. Muzahid 2014; Werk et al. 2014), is too low for *in situ* H_2 production. We thus speculate that the H_2 molecular gas is tidally stripped or ejected disk-material that retained a molecular phase partially due to self-shielding and the lower ambient UV radiation as suggested from simple photoionization models. The detections of molecular hydrogen in high velocity clouds (Richter et al. 2001) and in the leading arm of the Magellanic Stream (Sembach et al. 2001) reinforce such a scenario (see also Crighton et al. 2013).

Radio observations of the H I 21-cm line is another powerful tool for studying cold and neutral gas (Gupta et al. 2007, 2012) and diagnoses physical conditions in host-galaxies when detected (Gupta et al. 2013; Borthakur et al. 2014). The only system with $\rho < 10$ kpc (i.e. $z_{abs} = 0.10115$ towards Q 0439−433) shows a tentative detection of 21-cm absorption (Kanekar et al. 2001). Even in this case the QSO sight line is well beyond the stellar disk of the galaxy (Petitjean et al. 1996). A detailed analysis of this sys-

tem with follow up VLBA observations are presented in Dutta et al. (submitted).

It is apparent from Fig. 9 that the two systems showing the highest molecular fractions in our sample are detected at the largest impact parameters, i.e. $\rho \sim 80$ kpc. While H_2 producing cold gas is expected at low impact parameters (e.g. $\rho \lesssim 15$ kpc), systems at $\rho \sim 80$ kpc with a molecular fraction of $\sim 1/10$ are extremely surprising. The impact parameters for these two systems come from Oliveira et al. (2014, towards B0120-28) and Werk et al. (2013, towards J0925+4004). In addition to H_2, a detection of the HD molecule has been reported in the former system. We do not have the image of this field accessible to us to make any comment on the host-galaxy. However, we note that the molecular hydrogen is detected in four different components spread over ~ 180 km s^{-1}, implying a high volume filling factor of H_2 clouds in this absorber. Naively, one would expect such a case when a line-of-sight is passing through the stellar (or H I) disk of a galaxy, requiring a much lower impact parameter. In fact, for the two other systems in our sample showing multiple H_2 absorption components (i.e. $z_{abs} = 0.10115$ towards Q 0439–433 and $z_{abs} = 0.55733$ towards Q 0107–0232) show impact parameters of ~ 10 kpc. Therefore, this system is of particular interest for future deep observations. The later system is a part of the "COS-Halos" sample (Tumlinson et al. 2011; Werk et al. 2013), that were observed to investigate the circumgalactic medium of isolated L_* galaxies at $z \sim 0.2$. Nonetheless, we note that Werk et al. (2012) have found two candidate galaxies in the QSO J 0925+4004 field at the redshift of the absorber with impact parameters of 81 and 92 kpc respectively. This possibly could mean that the H_2 absorption is originating from a group environment and perhaps is not related to a halo of a single galaxy. We also note that two very faint photometric objects at $\rho \lesssim 20$ kpc, at the absorber's redshift, are seen in the SDSS image. Therefore, we can not rule out the possibility of one these objects being the true host-galaxy candidate. Deep images and determination of spectroscopic redshifts of all the photometric objects in this field are essential for understanding the true origin of molecular hydrogen in this system.

6 SUMMARY

We have conducted a systematic search for molecular hydrogen (H_2) in low redshift ($z < 0.7$) DLAs and sub-DLAs using the medium resolution HST/COS spectra that were available in the public HST archive before March, 2014. This is the first-ever systematic search for H_2 below the atmospheric cutoff. In total we found 33 DLAs/sub-DLAs with $\log N(\text{H I}) \gtrsim 19$, of which H_2 information is available for 27 systems. H_2 absorption from different rotational levels (up to $J = 3$) is seen in a total of 10/27 system with a $N(H_2)$ of $> 10^{14.4}$ cm^{-2}, 3/5 in DLAs and 7/22 in sub-DLAs. Three H_2 systems were reported previously by Crighton et al. (2013), Oliveira et al. (2014), and Srianand et al. (2014). The main findings of our analyses are summarized below:

● The H_2 detection rate, for $N(H_2) > 10^{14.4}$ cm^{-2}, in low-z DLAs/sub-DLAs is 50^{+25}_{-12} percent. This is a factor of $\gtrsim 2$ higher than that (i.e. 18^{+8}_{-4} percent) of the high-z sample of Noterdaeme et al. (2008a). We argue that the increase of the cosmic mean metallicity of DLAs/sub-DLAs and the dimming of the ambient radiation field intensity due to the decrease of the cosmic star-formation rate density, are responsible for the enhanced detection rate of molecular hydrogen at low-z.

• The median value of N(H I) for our sample is $10^{19.6}$ cm^{-2}. This is a factor of 10 lower than that of the N08 sample. Importantly, even with systematically lower N(H I) values, most of the low-z H$_2$ systems show a considerably large molecular fraction (i.e. $\log f_{H_2} \gtrsim -2.0$). This implies that either (a) the density is extremely high or (b) the radiation field is fairly weak in these H$_2$ absorbers. However, the absence of HD (and/or CO) molecules and the C I*, C II* absorption lines in the majority of the systems suggests that the density cannot be much higher than 10–100 cm^{-3}, as seen in the diffuse atomic phase of the Galactic ISM.

• Using simple photoionization models we show that the prevailing radiation field in the low-z H$_2$ systems is much weaker than the mean Galactic UV field for particle density in the range 10–100 cm^{-3}. The absence of higher-order rotational lines (i.e. $J \geqslant 4$) in all our H$_2$ systems provides independent evidence for the radiation field being weak. This indeed suggests that the H$_2$ bearing gas must be located far away from the star-forming luminous disk of the host galaxy.

• Eight out of 10 H$_2$ systems in our sample have host-galaxy information available from the literature. The majority of them (7/8) show impact parameters $\rho > 10$ kpc, suggesting that they perhaps do not originate from the luminous disks of the host-galaxies. We notice that even for the lowest impact parameter system (i.e. $\rho = 7.6$ kpc for the $z_{abs} = 0.10115$ towards Q 0439–433), the line of sight is outside the luminous stellar disk. Nonetheless, the possibility that these H$_2$ absorbers are actually originating in faint dwarf galaxies at much lower impact parameters, cannot be ruled out. Therefore, deep photometric searches for sub-L_* galaxies close to QSO lines of sight and follow up spectroscopic observations are indispensable for understanding the possible origin(s) of H$_2$ absorption in low-z DLAs/sub-DLAs.

• Low-z H$_2$ systems occupy a unique region in the $f_{H_2} - N_H$ plane (i.e. $\log f_{H_2} \gtrsim -4.5$ and $\log N$(H$_2$) $\lesssim 20.7$). Only a handful of H$_2$ systems from the high-z and the Galactic disk/Magellanic Cloud samples fall in this range of parameter-space. Interestingly, a significant fraction (i.e. 25/40) of the Galactic halo systems, with detected H$_2$, show similar range in f_{H_2} and N_H. This indicates that the physical conditions of molecular gas in low-z DLAs/sub-DLAs are, presumably, similar to those of the Milky Way halo gas.

• The f_{H_2} distribution for our low-z sample is significantly different compared to those of the Galactic disk/halo and the Magellanic Clouds (LMC/SMC) samples. Only a mild difference is noticed between the f_{H_2} distributions at low- and high-z for the entire sample. However, no difference is suggested when we consider only systems with $\log f_{H_2} > -4.9$. The mild difference inferred for the entire sample is the manifestation of the fact that the H$_2$ detection rate is considerably higher at low-z than at high-z.

• For the H$_2$ components with a total N(H$_2$) $> 10^{16.5}$ cm^{-2}, the median rotational excitation temperature is found to be $T_{01} = 133 \pm 55$ K. This is consistent with what has been seen in the "high-z DLAs" (e.g. 143±19 K). The inferred T_{01} are, however, slightly higher than those derived for the Galactic disk (i.e. 77±17 (rms) K, Savage et al. 1977), the Galactic halo (i.e. 115±13 K, Gillmon et al. 2006), and the Magellanic Clouds (i.e. 82±21 (rms) K, Tumlinson et al. 2002) systems.

• For further insight into the origin and nature of low-z DLAs/sub-DLAs, analyses based on observed metal lines and detailed ionization models will be presented elsewhere.

REFERENCES

Albornoz Vásquez, D., Rahmani, H., Noterdaeme, P., Petitjean, P., Srianand, R., & Ledoux, C., 2014, A&A, 562, A88

Bailly, D., Salumbides, E. J., Vervloet, M., & Ubachs, W., 2010, Molecular Physics, 108, 827

Balashev, S. A., Klimenko, V. V., Ivanchik, A. V., Varshalovich, D. A., Petitjean, P., & Noterdaeme, P., 2014, MNRAS, 440, 225

Battisti, A. J., Meiring, J. D., Tripp, T. M., et al., 2012, ApJ, 744, 93

Black, J. H., 1987, in Astrophysics and Space Science Library, Vol. 134, Interstellar Processes, Hollenbach, D. J. & Thronson, Jr., H. A., eds., pp. 731–744

Borthakur, S., Momjian, E., Heckman, T. M., York, D. G., Bowen, D. V., Yun, M. S., & Tripp, T. M., 2014, ApJ, 795, 98

Bouwens, R. J., Illingworth, G. D., Oesch, P. A., et al., 2011, ApJ, 737, 90

Christensen, L., Wisotzki, L., Roth, M. M., Sánchez, S. F., Kelz, A., & Jahnke, K., 2007, A&A, 468, 587

Crighton, N. H. M., Bechtold, J., Carswell, R. F., et al., 2013, MNRAS, 433, 178

Danforth, C. W., Stocke, J. T., & Shull, J. M., 2010, ApJ, 710, 613

Ferland, G. J., Porter, R. L., van Hoof, P. A. M., et al., 2013, Rev. Mexicana Astron. Astrofis., 49, 137

Fynbo, J. P. U., Laursen, P., Ledoux, C., et al., 2010, MNRAS, 408, 2128

Gehrels, N., 1986, ApJ, 303, 336

Ghavamian, P., Aloisi, A., Lennon, D., et al., 2009, Preliminary Characterization of the Post- Launch Line Spread Function of COS. Tech. rep.

Gillmon, K., Shull, J. M., Tumlinson, J., & Danforth, C., 2006, ApJ, 636, 891

Gould, R. J. & Salpeter, E. E., 1963, ApJ, 138, 393

Green, J. C., Froning, C. S., Osterman, S., et al., 2012, ApJ, 744, 60

Guimarães, R., Noterdaeme, P., Petitjean, P., Ledoux, C., Srianand, R., López, S., & Rahmani, H., 2012, AJ, 143, 147

Gupta, N., Srianand, R., Noterdaeme, P., Petitjean, P., & Muzahid, S., 2013, A&A, 558, A84

Gupta, N., Srianand, R., Petitjean, P., Bergeron, J., Noterdaeme, P., & Muzahid, S., 2012, A&A, 544, A21

Gupta, N., Srianand, R., Petitjean, P., Khare, P., Saikia, D. J., & York, D. G., 2007, ApJ, 654, L111

Haardt, F. & Madau, P., 1996, ApJ, 461, 20

—, 2001, in Clusters of Galaxies and the High Redshift Universe Observed in X-rays, Neumann, D. M. & Tran, J. T. V., eds.

—, 2012, ApJ, 746, 125

Hellsten, U., Hernquist, L., Katz, N., & Weinberg, D. H., 1998, ApJ, 499, 172

Hollenbach, D. & Salpeter, E. E., 1971, ApJ, 163, 155

Jenkins, E. B. & Peimbert, A., 1997, ApJ, 477, 265

Jorgenson, R. A., Murphy, M. T., Thompson, R., & Carswell, R. F., 2014, MNRAS, 443, 2783

Jorgenson, R. A. & Wolfe, A. M., 2014, ApJ, 785, 16

Kacprzak, G. G., Churchill, C. W., Evans, J. L., Murphy, M. T., & Steidel, C. C., 2011, MNRAS, 416, 3118

Kanekar, N., Chengalur, J. N., Subrahmanyan, R., & Petitjean, P., 2001, A&A, 367, 46

Kriss, G. A., 2011, Improved Medium Resolution Line Spread Functions for COS FUV Spectra. Tech. rep.

Kulkarni, V. P., Fall, S. M., Lauroesch, J. T., York, D. G., Welty, D. E., Khare, P., & Truran, J. W., 2005, ApJ, 618, 68

Kulkarni, V. P., Khare, P., Péroux, C., York, D. G., Lauroesch, J. T., & Meiring, J. D., 2007, ApJ, 661, 88

Kulkarni, V. P., Woodgate, B. E., York, D. G., Thatte, D. G., Meiring, J., Palunas, P., & Wassell, E., 2006, ApJ, 636, 30

Lanzetta, K. M., Wolfe, A. M., Altan, H., et al., 1997, AJ, 114, 1337

Ledoux, C., Petitjean, P., Fynbo, J. P. U., Møller, P., & Srianand, R., 2006a, A&A, 457, 71

Ledoux, C., Petitjean, P., & Srianand, R., 2003, MNRAS, 346, 209

—, 2006b, ApJ, 640, L25

Meiring, J. D., Tripp, T. M., Prochaska, J. X., et al., 2011, ApJ, 732, 35

Meiring, J. D., Tripp, T. M., Werk, J. K., Howk, J. C., Jenkins, E. B., Prochaska, J. X., Lehner, N., & Sembach, K. R., 2013, ApJ, 767, 49

Møller, P., Fynbo, J. P. U., & Fall, S. M., 2004, A&A, 422, L33

Muzahid, S., 2014, ApJ, 784, 5

Noterdaeme, P., Laursen, P., Petitjean, P., et al., 2012a, A&A, 540, A63

Noterdaeme, P., Ledoux, C., Petitjean, P., & Srianand, R., 2008a, A&A, 481, 327

Noterdaeme, P., Ledoux, C., Srianand, R., Petitjean, P., & Lopez, S., 2009a, A&A, 503, 765

Noterdaeme, P., Petitjean, P., Carithers, W. C., et al., 2012b, A&A, 547, L1

Noterdaeme, P., Petitjean, P., Ledoux, C., López, S., Srianand, R., & Vergani, S. D., 2010, A&A, 523, A80

Noterdaeme, P., Petitjean, P., Ledoux, C., & Srianand, R., 2009b, A&A, 505, 1087

Noterdaeme, P., Petitjean, P., Ledoux, C., Srianand, R., & Ivanchik, A., 2008b, A&A, 491, 397

Noterdaeme, P., Petitjean, P., Srianand, R., Ledoux, C., & Le Petit, F., 2007, A&A, 469, 425

Oliveira, C. M., Sembach, K. R., Tumlinson, J., O'Meara, J., & Thom, C., 2014, ApJ, 783, 22

Osterman, S., Green, J., Froning, C., et al., 2011, Ap&SS, 335, 257

Péroux, C., Bouché, N., Kulkarni, V. P., York, D. G., & Vladilo, G., 2011, MNRAS, 410, 2237

Péroux, C., Dessauges-Zavadsky, M., D'Odorico, S., Kim, T.-S., & McMahon, R. G., 2003a, MNRAS, 345, 480

Péroux, C., McMahon, R. G., Storrie-Lombardi, L. J., & Irwin, M. J., 2003b, MNRAS, 346, 1103

Petitjean, P., Ledoux, C., Noterdaeme, P., & Srianand, R., 2006, A&A, 456, L9

Petitjean, P., Srianand, R., & Ledoux, C., 2002, MNRAS, 332, 383

Petitjean, P., Theodore, B., Smette, A., & Lespine, Y., 1996, A&A, 313, L25

Pettini, M., Smith, L. J., King, D. L., & Hunstead, R. W., 1997, ApJ, 486, 665

Prochaska, J. X., Gawiser, E., Wolfe, A. M., Castro, S., & Djorgovski, S. G., 2003, ApJ, 595, L9

Prochaska, J. X. & Wolfe, A. M., 2009, ApJ, 696, 1543

Rafelski, M., Wolfe, A. M., Prochaska, J. X., Neeleman, M., & Mendez, A. J., 2012, ApJ, 755, 89

Rao, S. M., Belfort-Mihalyi, M., Turnshek, D. A., Monier, E. M., Nestor, D. B., & Quider, A., 2011, MNRAS, 416, 1215

Rao, S. M., Turnshek, D. A., & Nestor, D. B., 2006, ApJ, 636, 610

Reimers, D., Baade, R., Quast, R., & Levshakov, S. A., 2003, A&A, 410, 785

Richter, P., Sembach, K. R., Wakker, B. P., & Savage, B. D., 2001, ApJ, 562, L181

Rodríguez, E., Petitjean, P., Aracil, B., Ledoux, C., & Srianand, R., 2006, A&A, 446, 791

Roy, N., Chengalur, J. N., & Srianand, R., 2006, MNRAS, 365, L1

Savage, B. D., Bohlin, R. C., Drake, J. F., & Budich, W., 1977, ApJ, 216, 291

Savage, B. D., Narayanan, A., Lehner, N., & Wakker, B. P., 2011, ApJ, 731, 14

Schaye, J., Aguirre, A., Kim, T.-S., Theuns, T., Rauch, M., & Sargent, W. L. W., 2003, ApJ, 596, 768

Sembach, K. R., Howk, J. C., Savage, B. D., & Shull, J. M., 2001, AJ, 121, 992

Snow, T. P., Rachford, B. L., Tumlinson, J., et al., 2000, ApJ, 538, L65

Som, D., Kulkarni, V. P., Meiring, J., York, D. G., Péroux, C., Khare, P., & Lauroesch, J. T., 2013, MNRAS, 435, 1469

Srianand, R., Noterdaeme, P., Ledoux, C., & Petitjean, P., 2008, A&A, 482, L39

Srianand, R., Petitjean, P., Ledoux, C., Ferland, G., & Shaw, G., 2005, MNRAS, 362, 549

Srianand, R., Rahmani, H., Muzahid, S., & Mohan, V., 2014, MNRAS, 443, 3318

Tejos, N., Morris, S. L., Finn, C. W., et al., 2014, MNRAS, 437, 2017

Tremonti, C. A., Heckman, T. M., Kauffmann, G., et al., 2004, ApJ, 613, 898

Tripp, T. M., Jenkins, E. B., Bowen, D. V., Prochaska, J. X., Aracil, B., & Ganguly, R., 2005, ApJ, 619, 714

Tumlinson, J., Malec, A. L., Carswell, R. F., et al., 2010, ApJ, 718, L156

Tumlinson, J., Shull, J. M., Rachford, B. L., et al., 2002, ApJ, 566, 857

Tumlinson, J., Werk, J. K., Thom, C., et al., 2011, ApJ, 733, 111

Welty, D. E., Xue, R., & Wong, T., 2012, ApJ, 745, 173

Werk, J. K., Prochaska, J. X., Thom, C., Tumlinson, J., Tripp, T. M., O'Meara, J. M., & Meiring, J. D., 2012, ApJS, 198, 3

Werk, J. K., Prochaska, J. X., Thom, C., Tumlinson, J., Tripp, T. M., O'Meara, J. M., & Peeples, M. S., 2013, ApJS, 204, 17

Werk, J. K., Prochaska, J. X., Tumlinson, J., et al., 2014, ApJ, 792, 8

Wolfe, A. M., Gawiser, E., & Prochaska, J. X., 2005, ARA&A, 43, 861

Wolfe, A. M. & Prochaska, J. X., 1998, ApJ, 494, L15

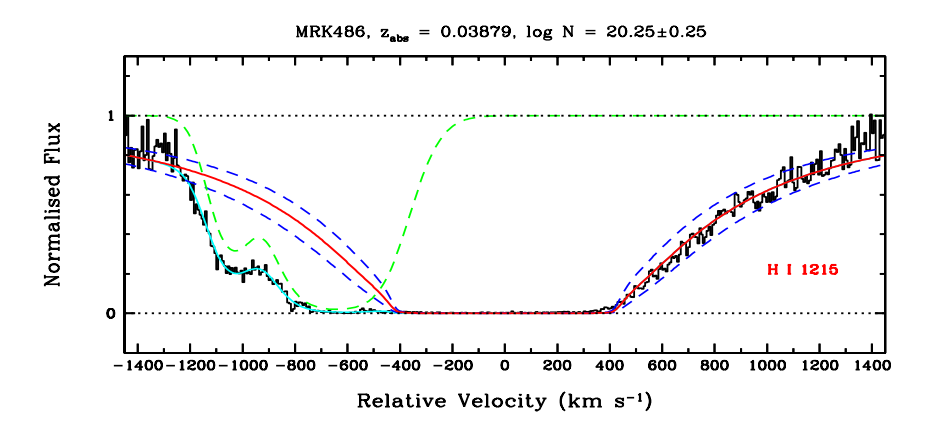**APPENDIX A: VOIGT PROFILE FIT TO H I ABSORPTION LINES FOR SYSTEMS LISTED IN TABLE 1**

MRK486, $z_{\rm abs}$ = 0.03879, log N = 20.25±0.25

Figure A1. Damped Lyα absorption from $z_{\rm abs}$ = 0.03879 towards MRK486 system. The red smooth and blue dashed curves plotted on the data (black histogram) are the best fitting Voigt profiles for the sub-DLA component and its 1σ uncertainty. Unrelated absorption is usually fitted assuming Lyα. The green dashed curve at ~ 800 km s^{-1} shows an unrelated absorption. Cyan curve represents the total (sub-DLA + unrelated) absorption model.

Q0439−433, $z_{\rm abs}$ = 0.10115, log N = 19.63±0.08
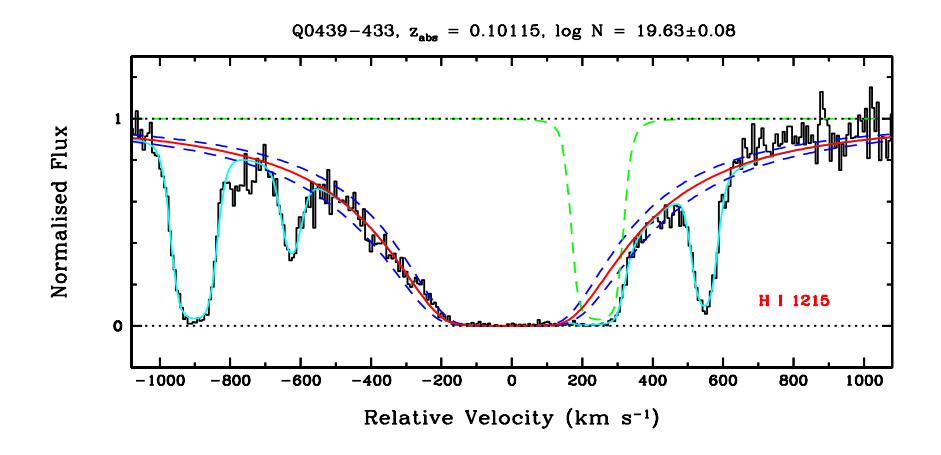
Figure A2. Sub-damped Lyα absorption from $z_{\rm abs}$ = 0.10115 towards Q 0439-433 system. Various curves are as described in Fig. A1.

PHL1226, $z_{\rm abs}$ = 0.15962, log N = 19.37±0.10
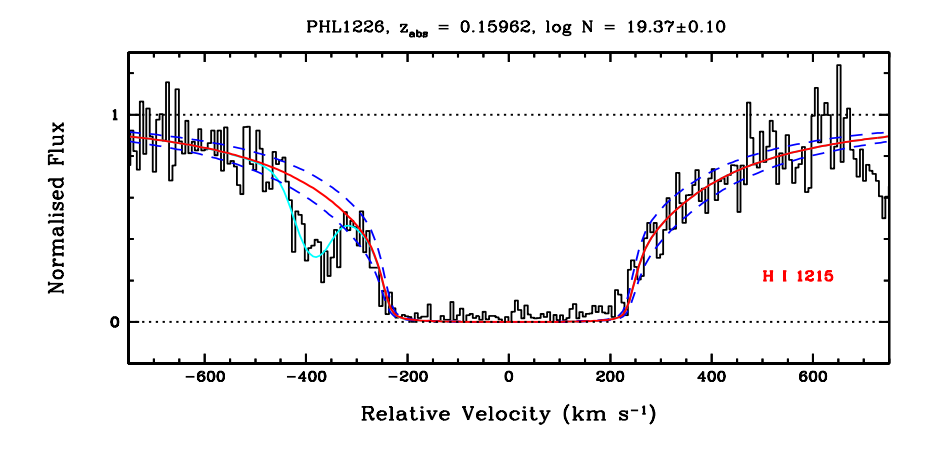
Figure A3. Sub-damped Lyα absorption from $z_{\rm abs}$ = 0.15962 towards PHL1226 system. Various curves are as described in Fig. A1.

Q0850+440, $z_{\rm abs}$ = 0.16375, log N = 19.67±0.10

H I 937

H I 949

H I 972

H I 1025
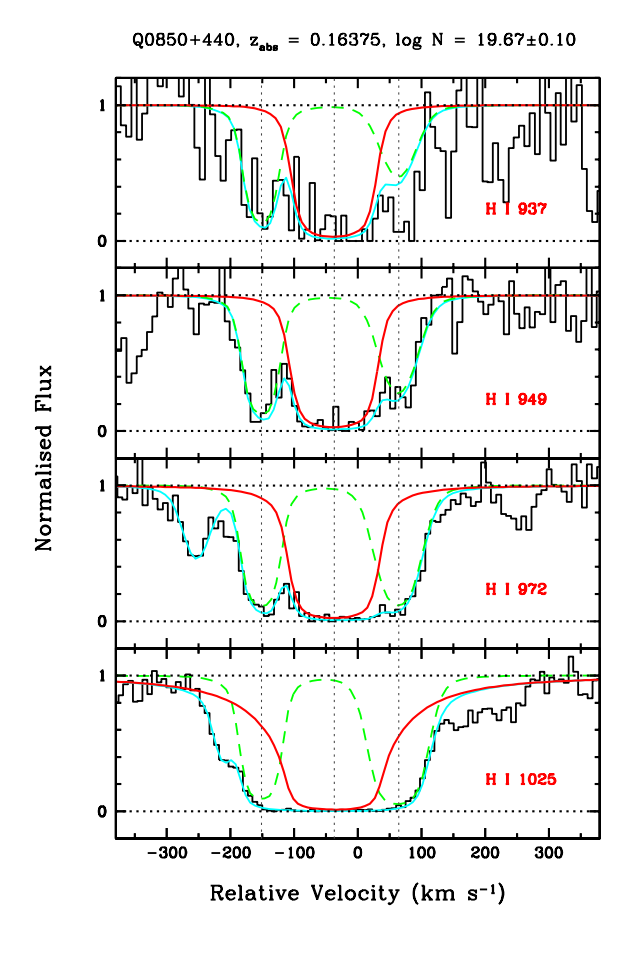
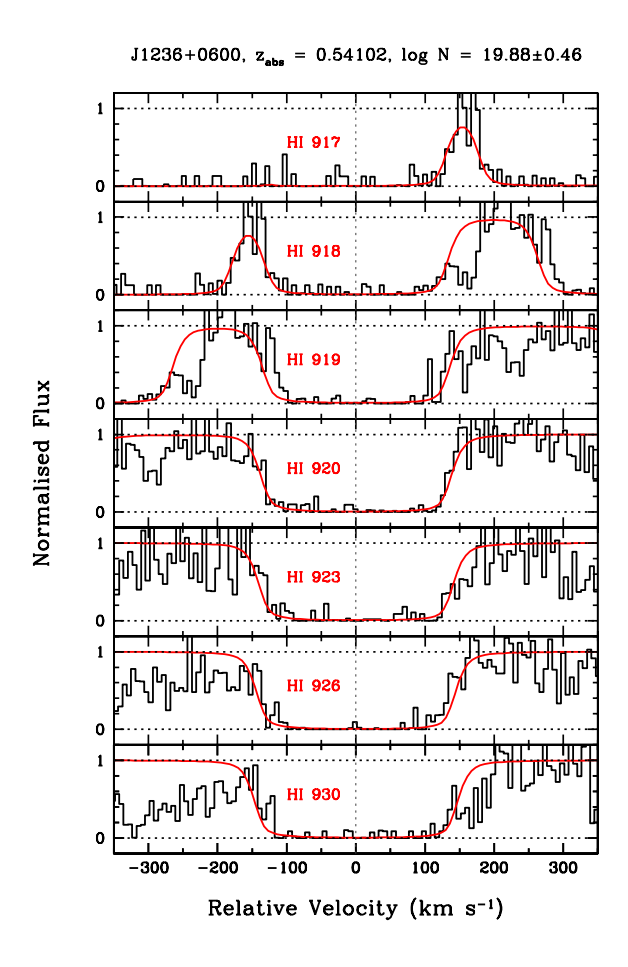**Figure A4.** Lyman series absorption from $z_{\rm abs}$ = 0.16375 towards Q 0850+440 system. Various curves are as described in Fig. A1.

Q1323+343, $z_{\rm abs}$ = 0.35300, log N = 18.92±0.20

H I 1215
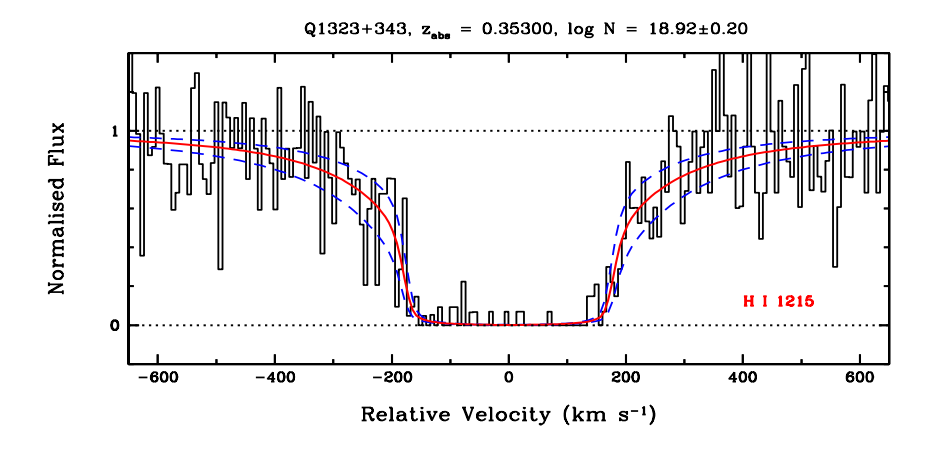
Figure A5. Sub-damped Lyα absorption from $z_{\rm abs}$ = 0.35300 towards Q1323+343 system. Various curves are as described in Fig. A1.

Q1400+553, z$_{abs}$ = 0.36475, log N = 20.11±0.20
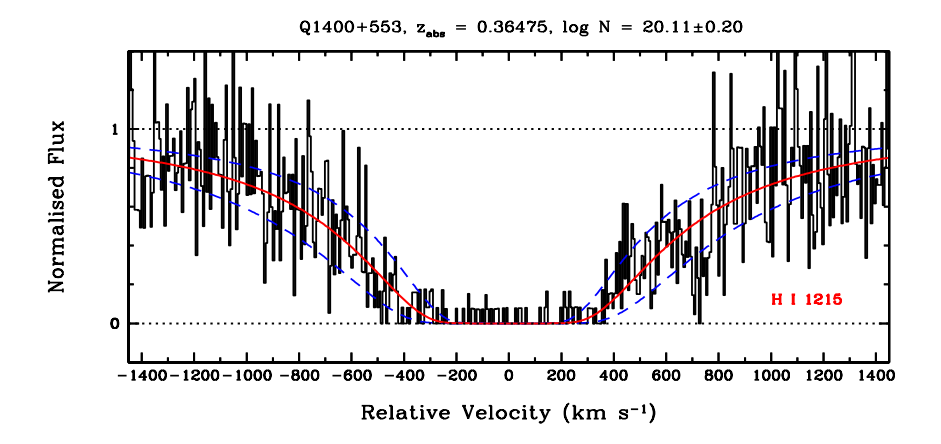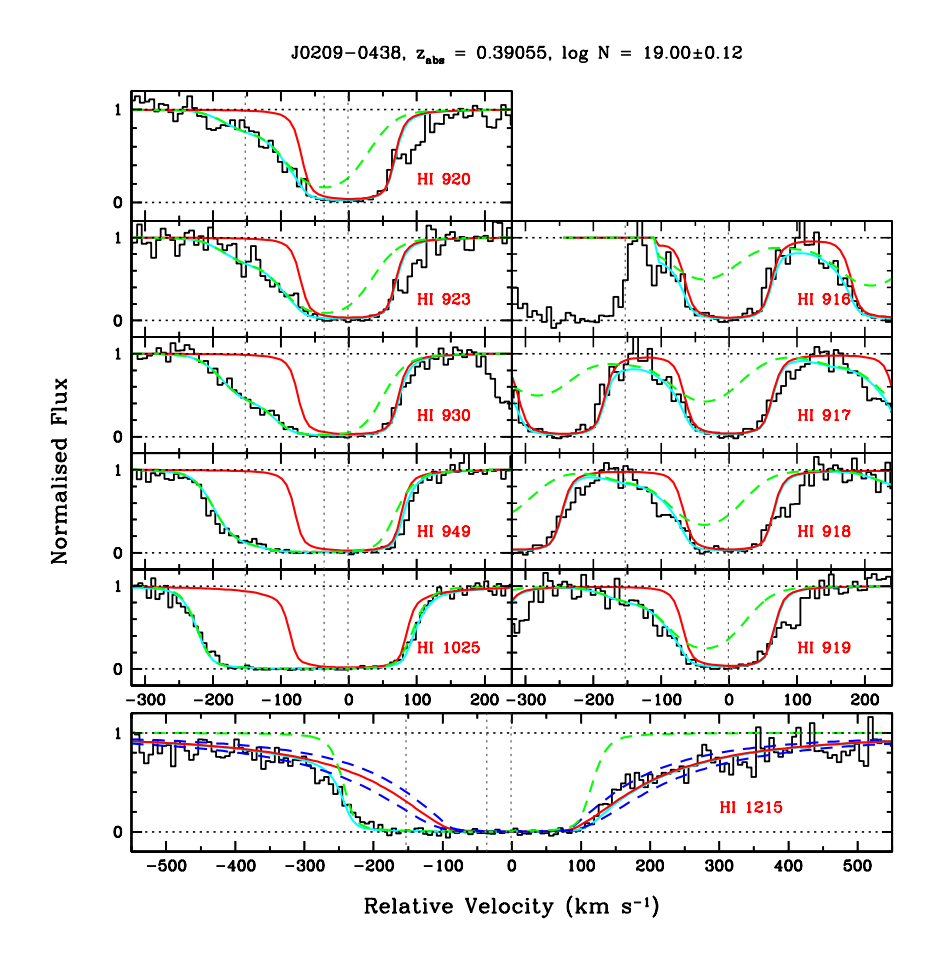
Figure A6. Damped Lyα absorption from z_{abs} = 0.36475 towards Q1400+553 system. Various curves are as described in Fig. A1.

J0209−0438, z$_{abs}$ = 0.39055, log N = 19.00±0.12

Figure A7. Lyman series absorption from z_{abs} = 0.39055 towards J0209-0438 system. Various curves are as described in Fig. A1.

Q1232−022, $z_{\rm abs}$ = 0.39495, log N = 20.79±0.20

H I 1025

H I 1215

Relative Velocity (km s⁻¹)
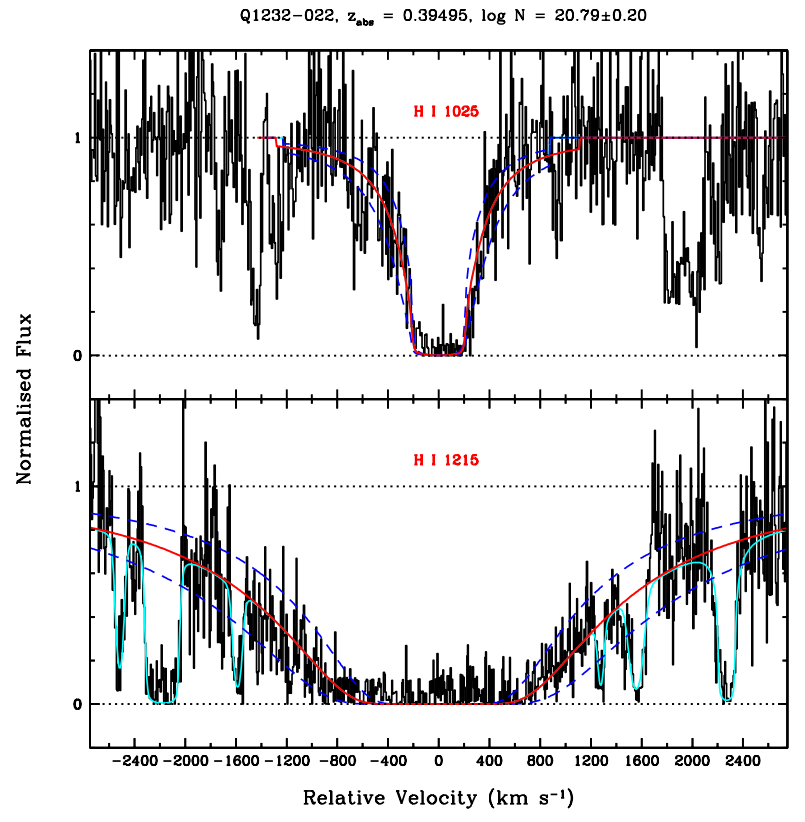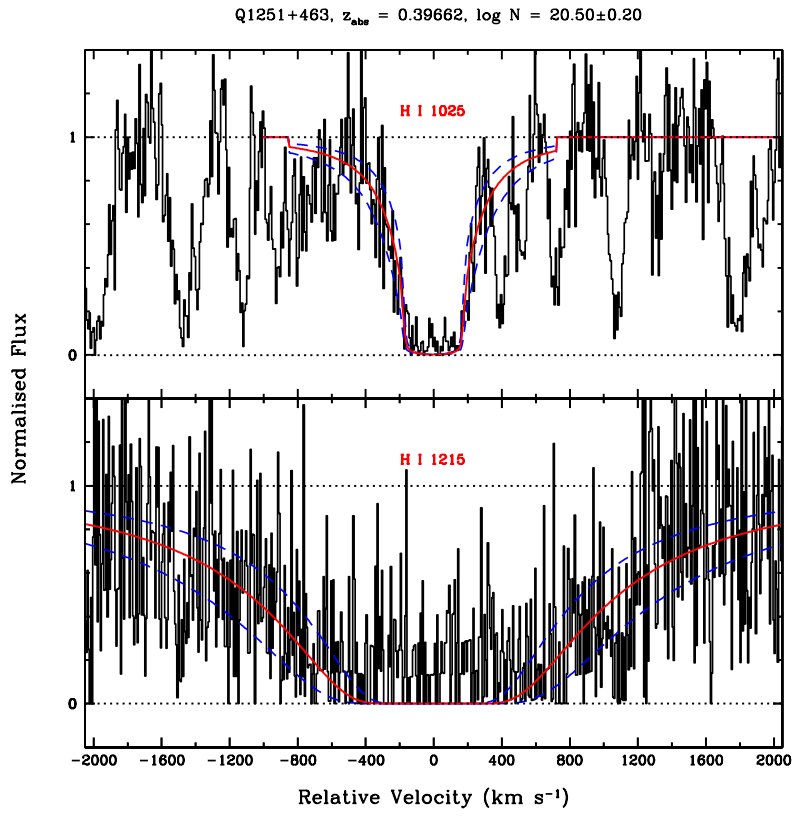
Figure A8. Damped Lyα and Lyβ absorption from $z_{\rm abs} = 0.39495$ towards Q1232−022 system. Various curves are as described in Fig. A1.

Q1251+463, $z_{\rm abs}$ = 0.39662, log N = 20.50±0.20

H I 1025

H I 1215

Relative Velocity (km s⁻¹)

Figure A9. Damped Lyα and Lyβ absorption from $z_{\rm abs} = 0.39662$ towards Q1251+463 system. Various curves are as described in Fig. A1.

Q0454−2203, z_abs = 0.47437, log N = 19.97±0.15
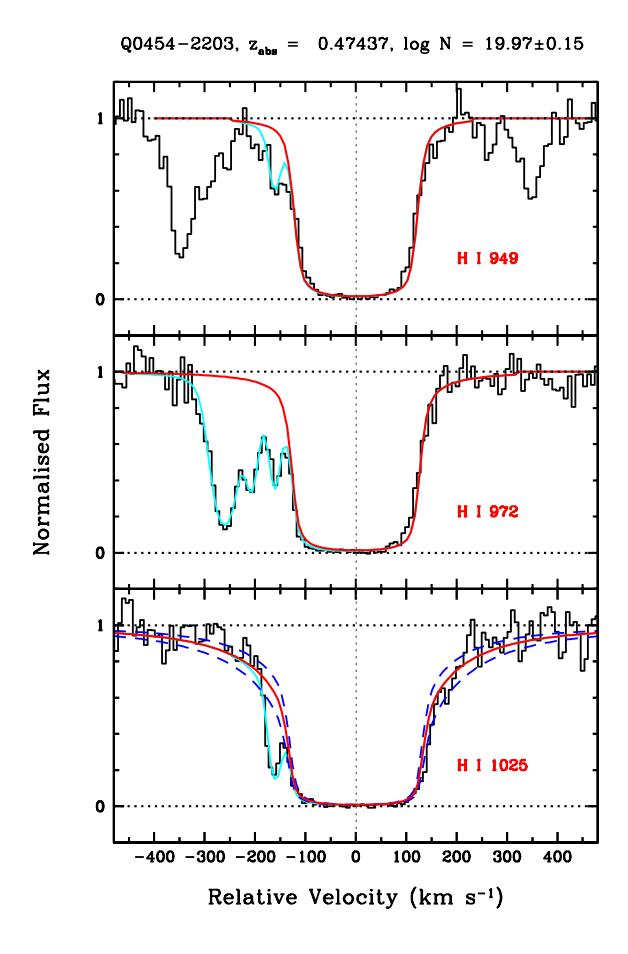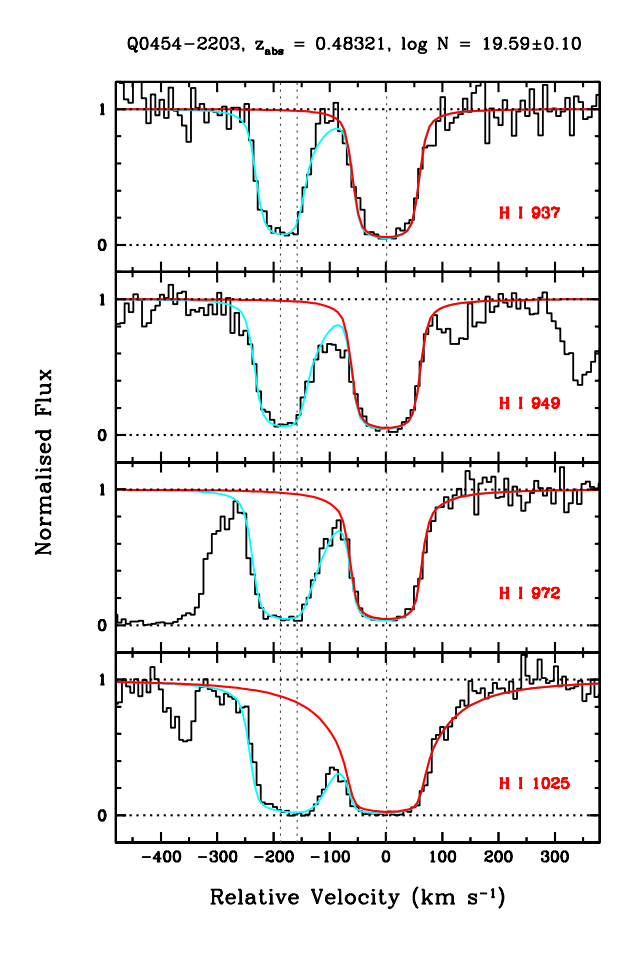
Figure A10. Lyman series absorption from $z_{\rm abs}$ = 0.47437 towards Q0454-2203 system. Various curves are as described in Fig. A1.

Q0454−2203, $z_{\rm abs}$ = 0.48321, log N = 19.59±0.10

H I 937

H I 949

H I 972

H I 1025

Normalised Flux

Relative Velocity (km s^{-1})

Figure A11. Lyman series absorption from $z_{\rm abs}$ = 0.48321 towards Q0454-2203 system. Various curves are as described in Fig. A1.
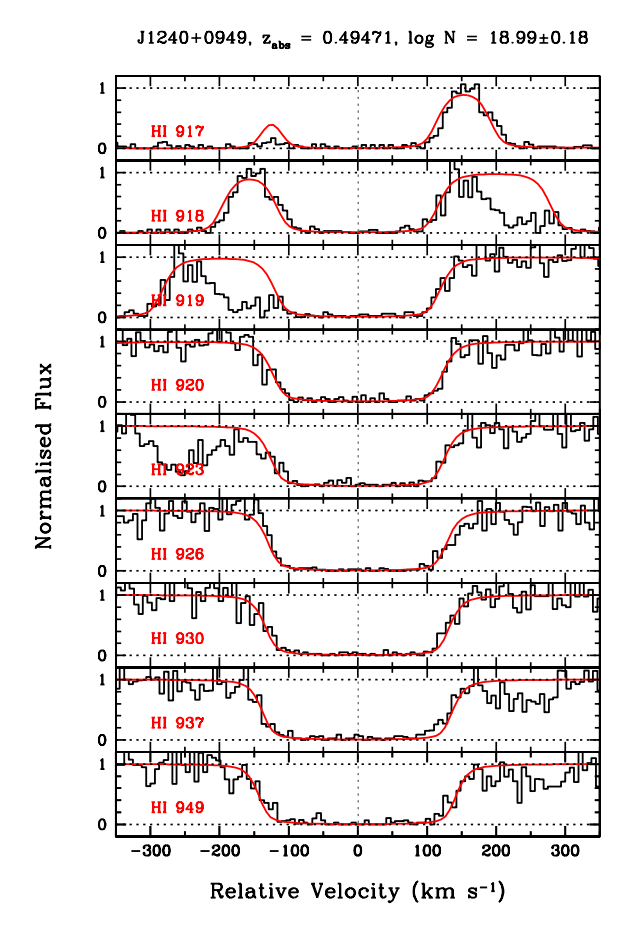
Figure A12. Lyman series absorption from $z_{\rm abs} = 0.49471$ towards J1240+0949 system. Various curves are as described in Fig. A1.

J1236+0600, z_{abs} = 0.54102, log N = 19.88±0.46

HI 917

HI 918

HI 919

HI 920

HI 923

HI 926

HI 930

Normalised Flux

Relative Velocity (km s⁻¹)

Figure A13. Lyman series absorption from z_{abs} = 0.54102 towards J1236+0600 system. Various curves are as described in Fig. A1.

Q1317+227, $z_{\rm abs}$ = 0.66047, log N = 19.65±0.10
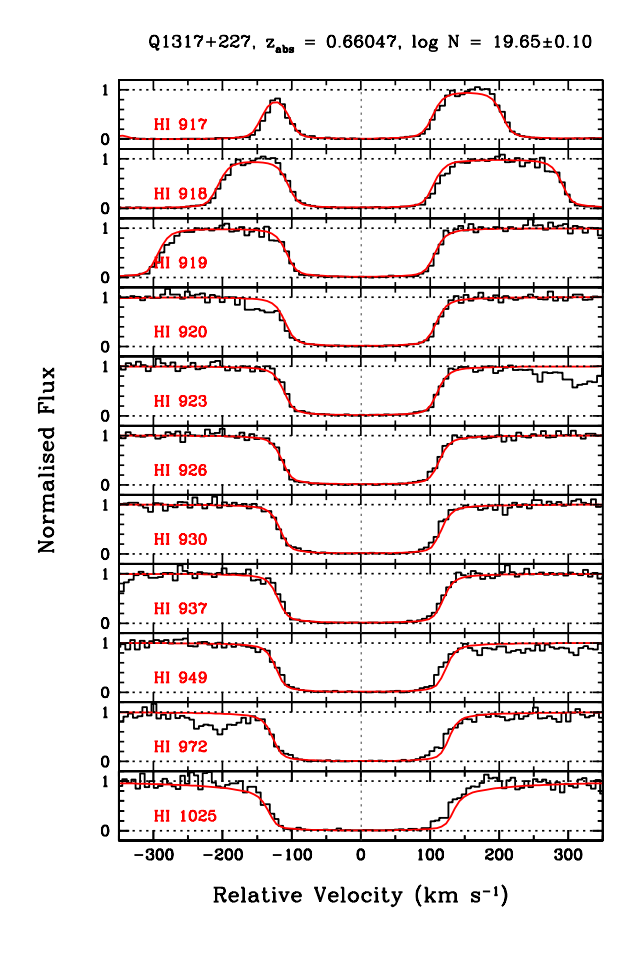
Figure A14. Lyman series absorption from $z_{\rm abs}$ = 0.66047 towards Q1317+227 system. Various curves are as described in Fig. A1.

APPENDIX B: VOIGT PROFILE FIT TO H I ABSORPTION LINES FOR SYSTEMS LISTED IN TABLE 2

J1407+5507, $z_{\rm abs}$ = 0.00474, log N = 19.75±0.05
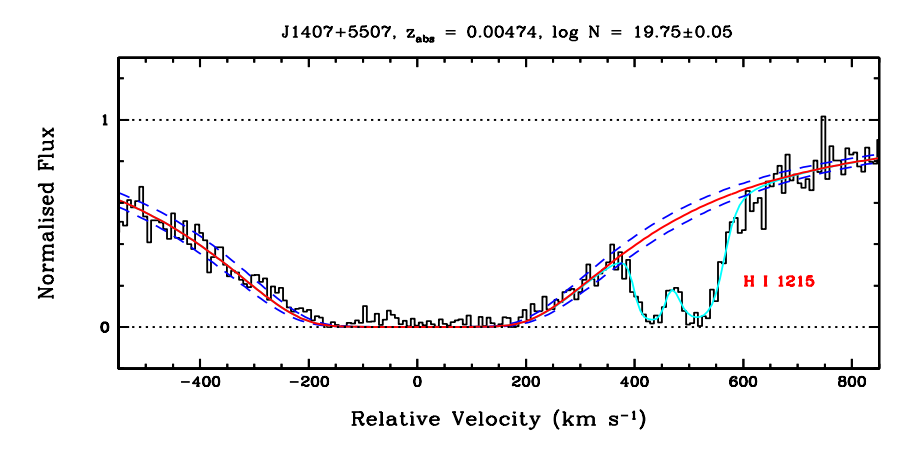
Figure B1. Sub-damped Lyα absorption from $z_{\rm abs}$ = 0.00474 towards J1407+5507 system. The blue wing is affected by the Galactic Lyα absorption. Various curves are as described in Fig. A1.
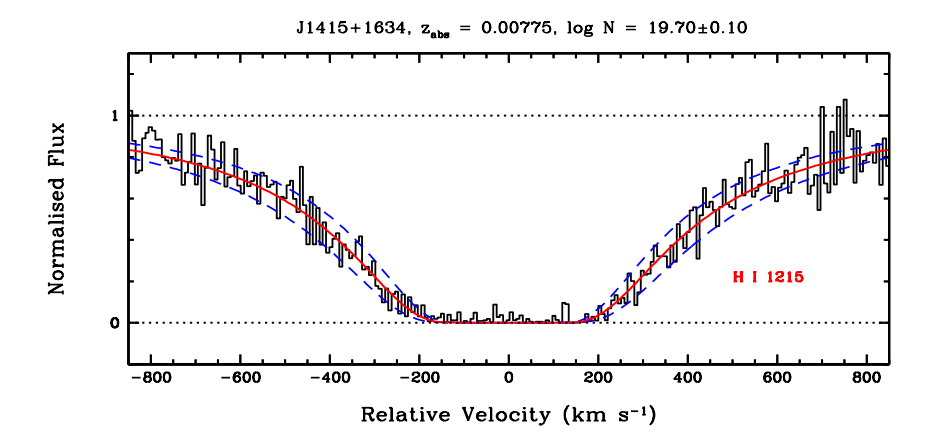
Figure B2. Sub-damped Lyα absorption from $z_{\text{abs}} = 0.00775$ towards J1415+1634 system. Various curves are as described in Fig. A1.
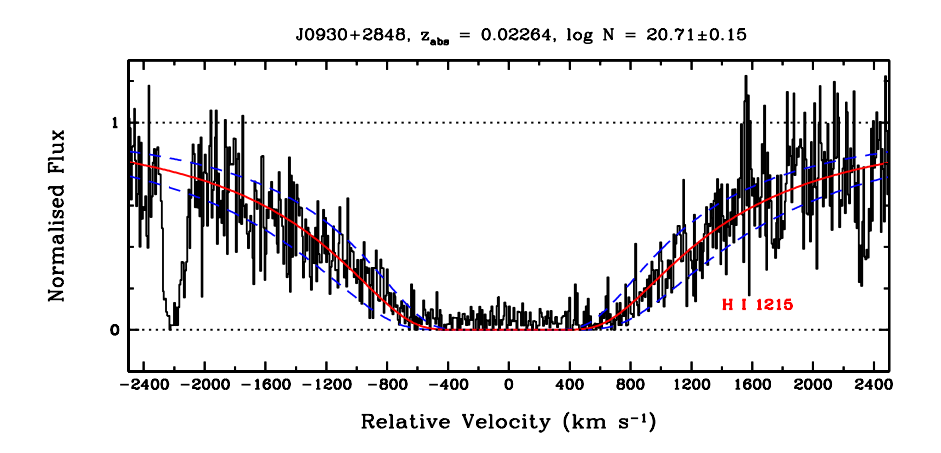
Figure B3. Damped Lyα absorption from $z_{\text{abs}} = 0.02264$ towards J0930+2848 system. Various curves are as described in Fig. A1.
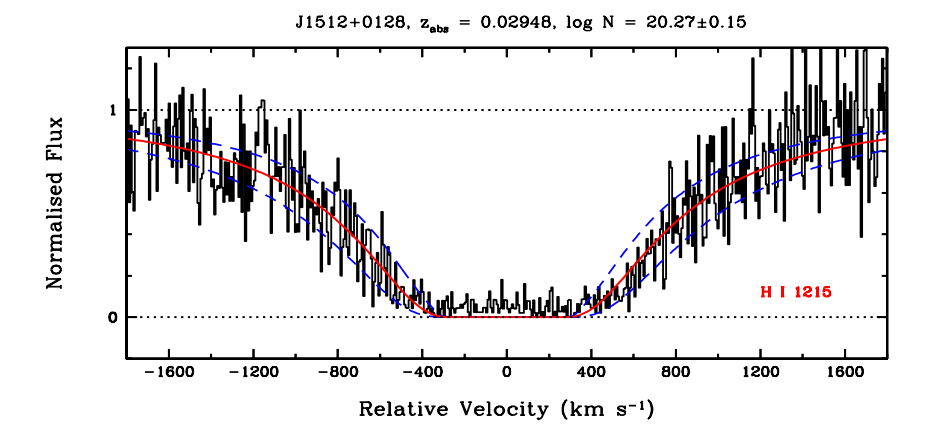
Figure B4. Damped Lyα absorption from $z_{\text{abs}} = 0.02948$ towards J1512+0128 system. Various curves are as described in Fig. A1.
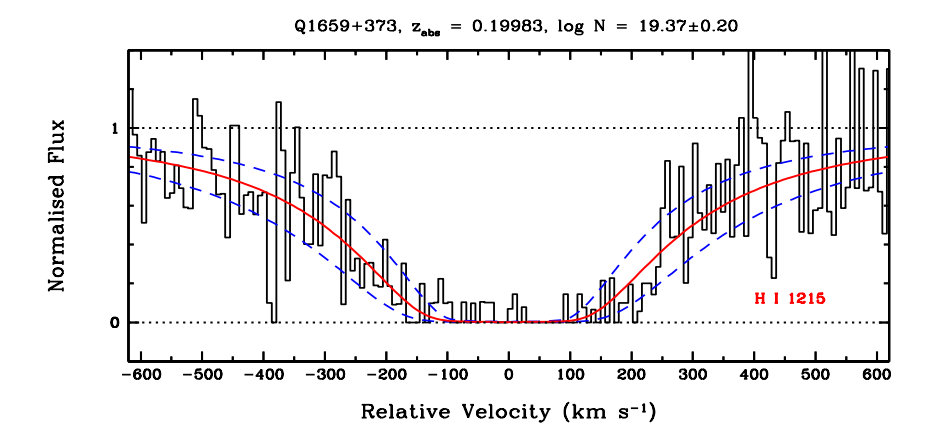
Figure B5. Sub-damped Lyα absorption from $z_{\rm abs} = 0.19983$ towards Q1659+373 system. Various curves are as described in Fig. A1.

APPENDIX C: VOIGT PROFILE FIT TO MOLECULAR HYDROGEN ABSORPTION
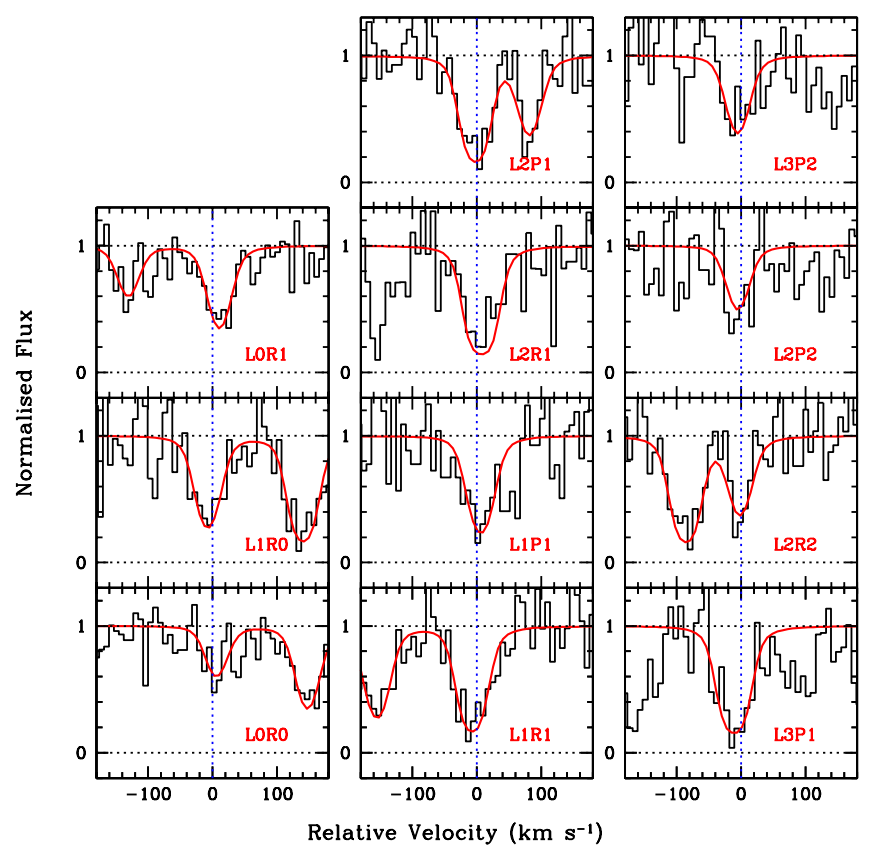
Figure C1. Molecular hydrogen absorption from the $z_{\rm abs} = 0.06650$ towards J1241+2852 system. The red smooth curves are the best fitting Voigt profiles to the data (in black histogram). The vertical dotted line marks the median line centroid.
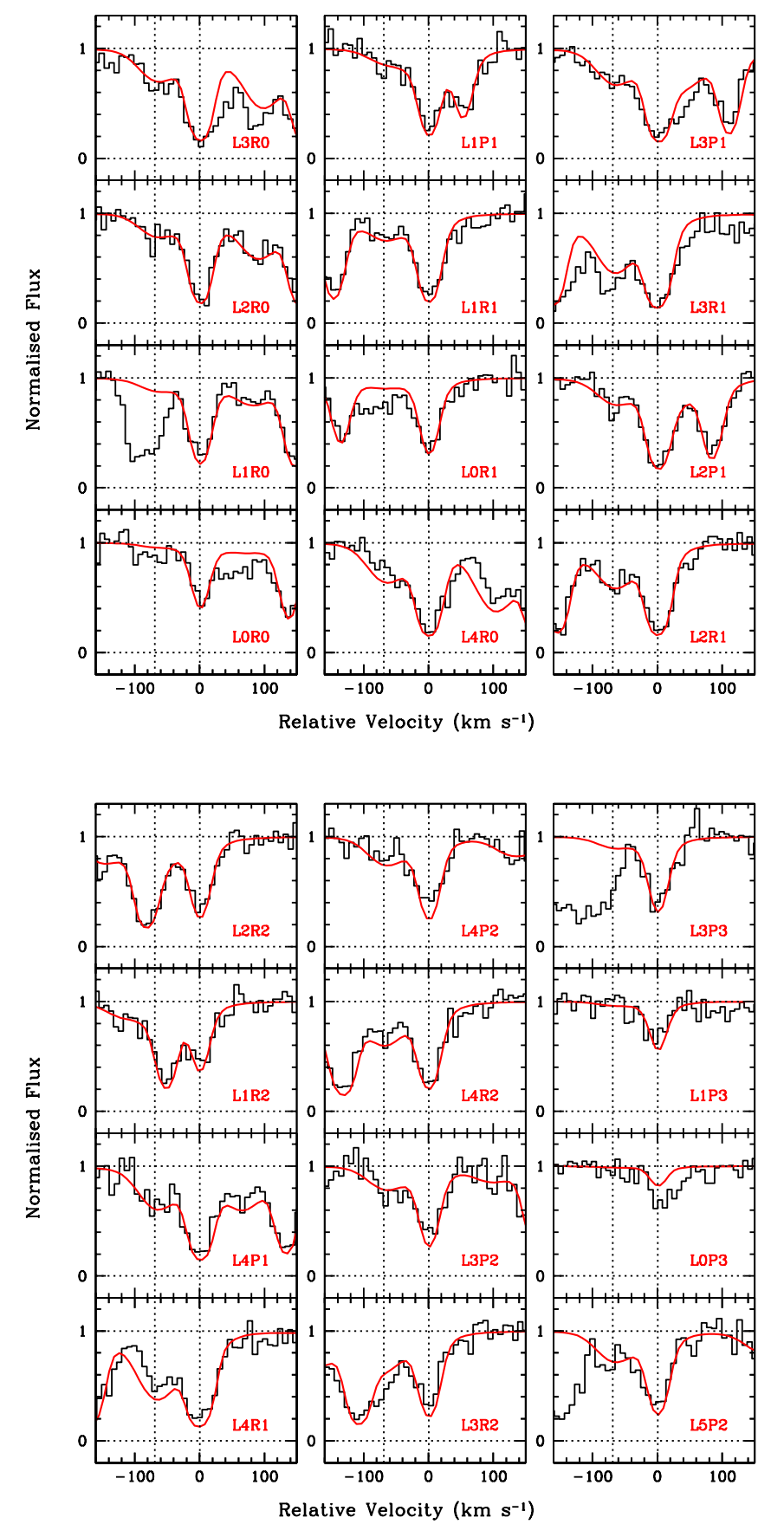
Figure C2. Molecular hydrogen absorption from the $z_{abs} = 0.10115$ towards Q0439–433 system. A weak component is possibly detected at ~ 70 km s^{-1}.

Figure C2. Continued.
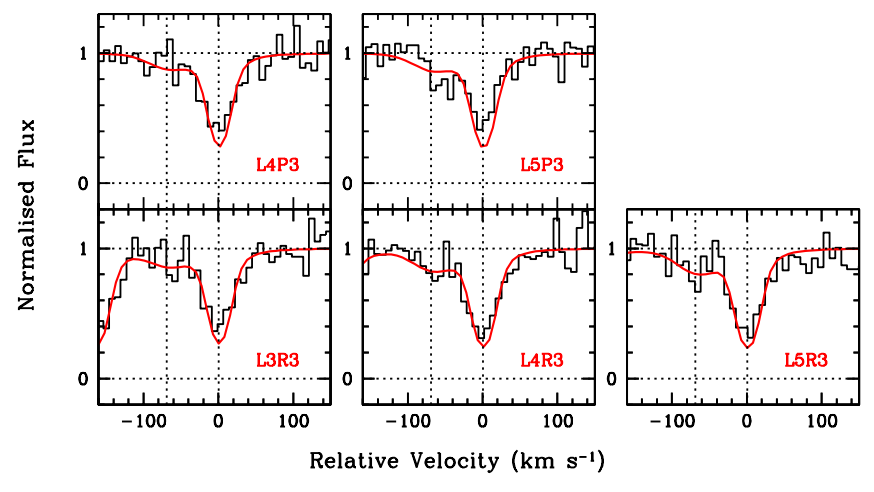
Figure C3. Molecular hydrogen absorption from the $z_{abs} = 0.16375$ towards Q0850+440 system. Note that both the L3R0 $\lambda 1062.8$ and L3R1 $\lambda 1063.4$ lines fall at the edge of the detector segment "B" and are shifted towards blue by slightly more than 20 km s^{-1}.
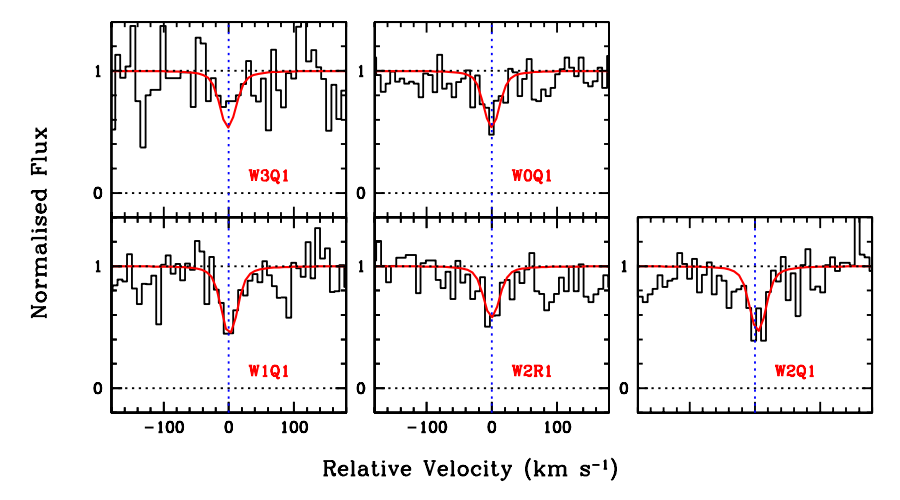
Figure C4. Molecular hydrogen absorption from the $z_{\rm abs} = 0.22711$ towards J1342–0053 system.
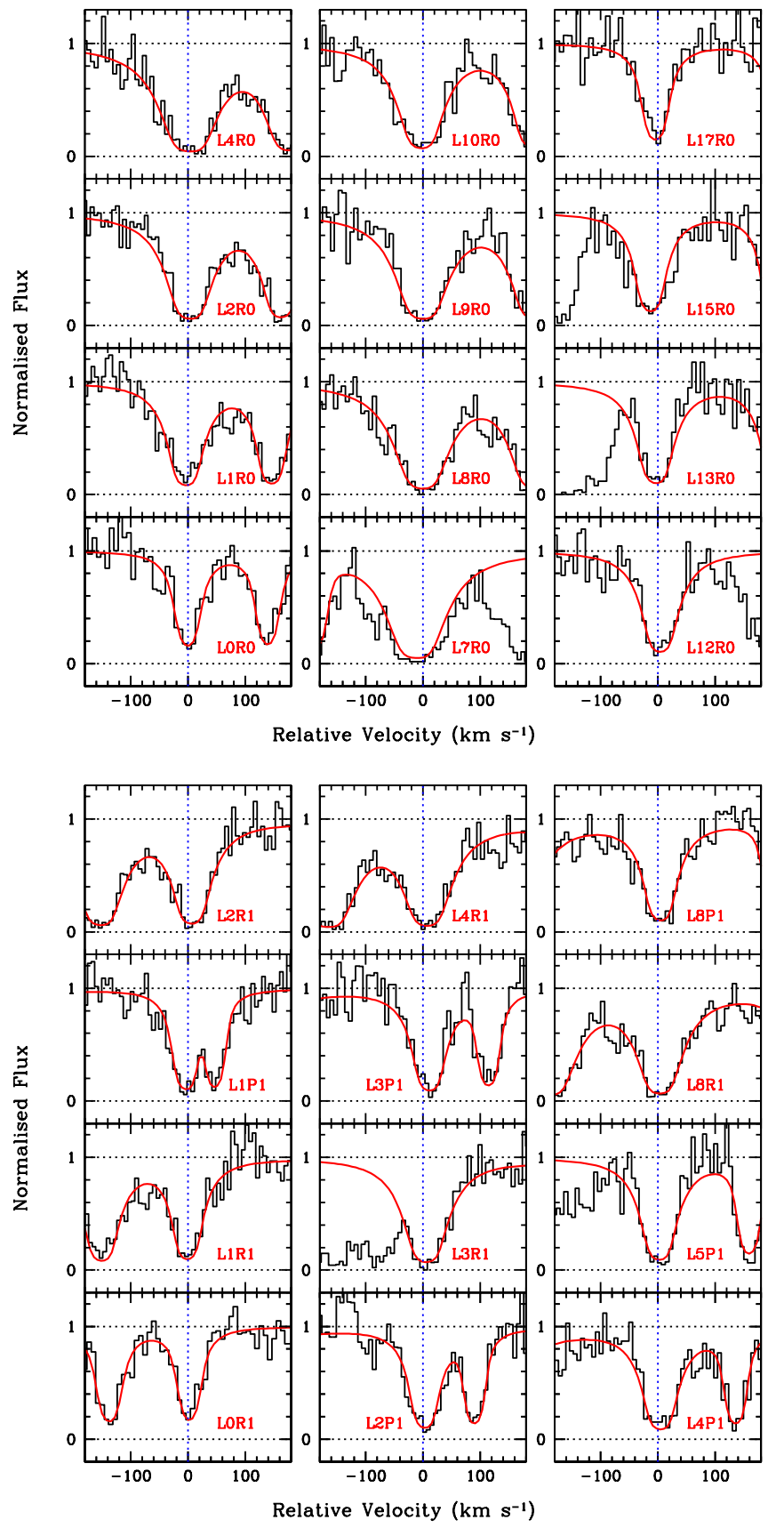
Figure C5. Molecular hydrogen absorption from the $z_{abs} = 0.32110$ towards J1616+4154 system.

Figure C5. Continued.
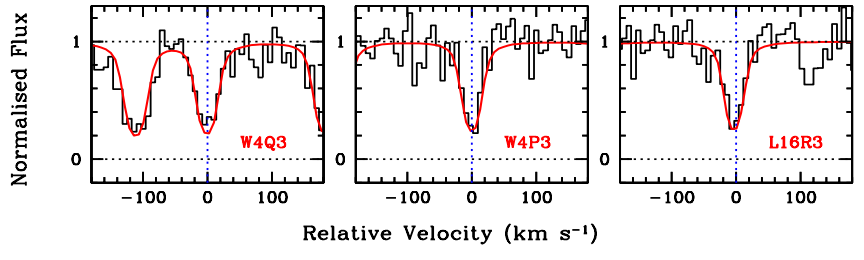
Figure C5. Continued.
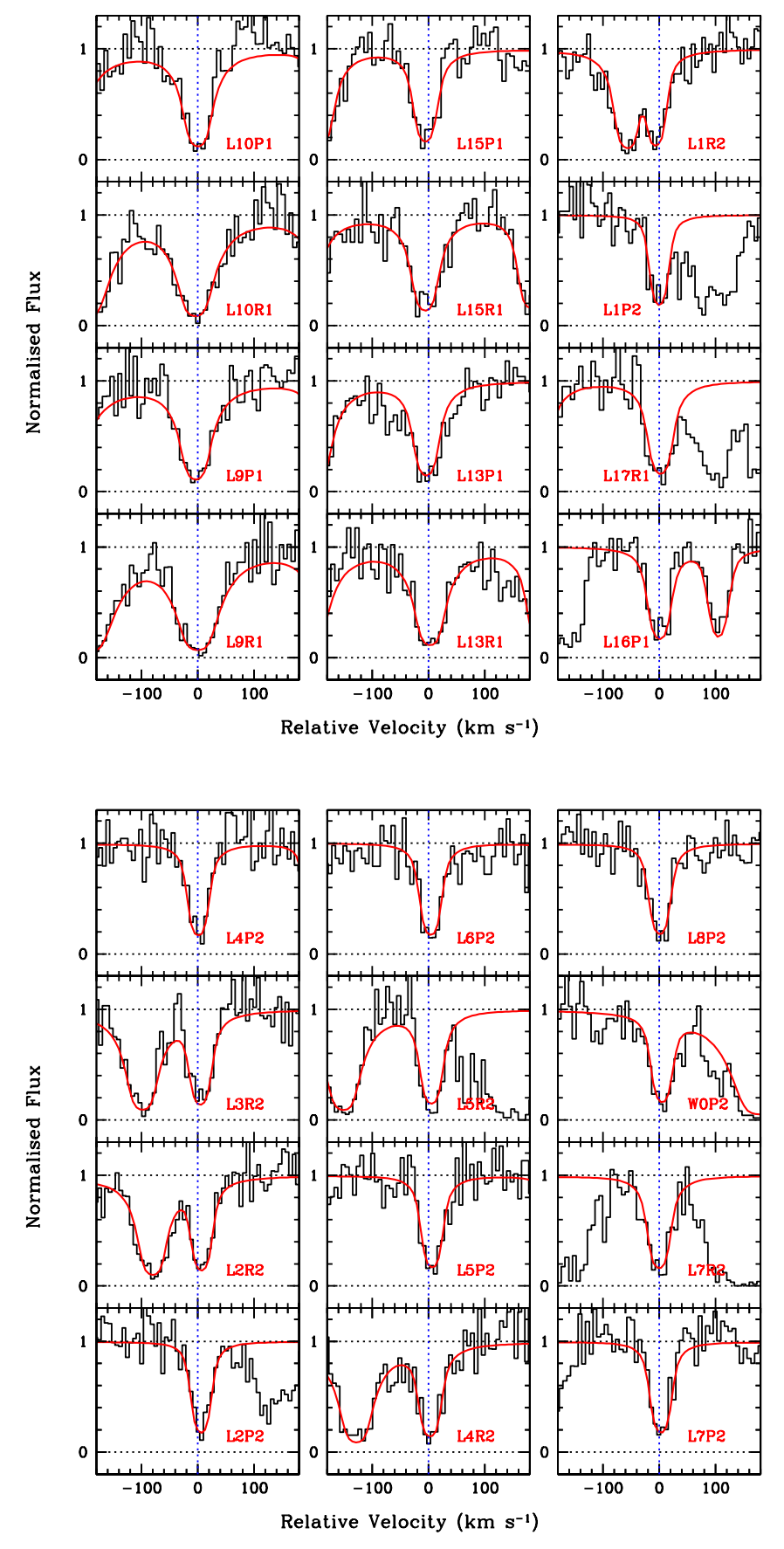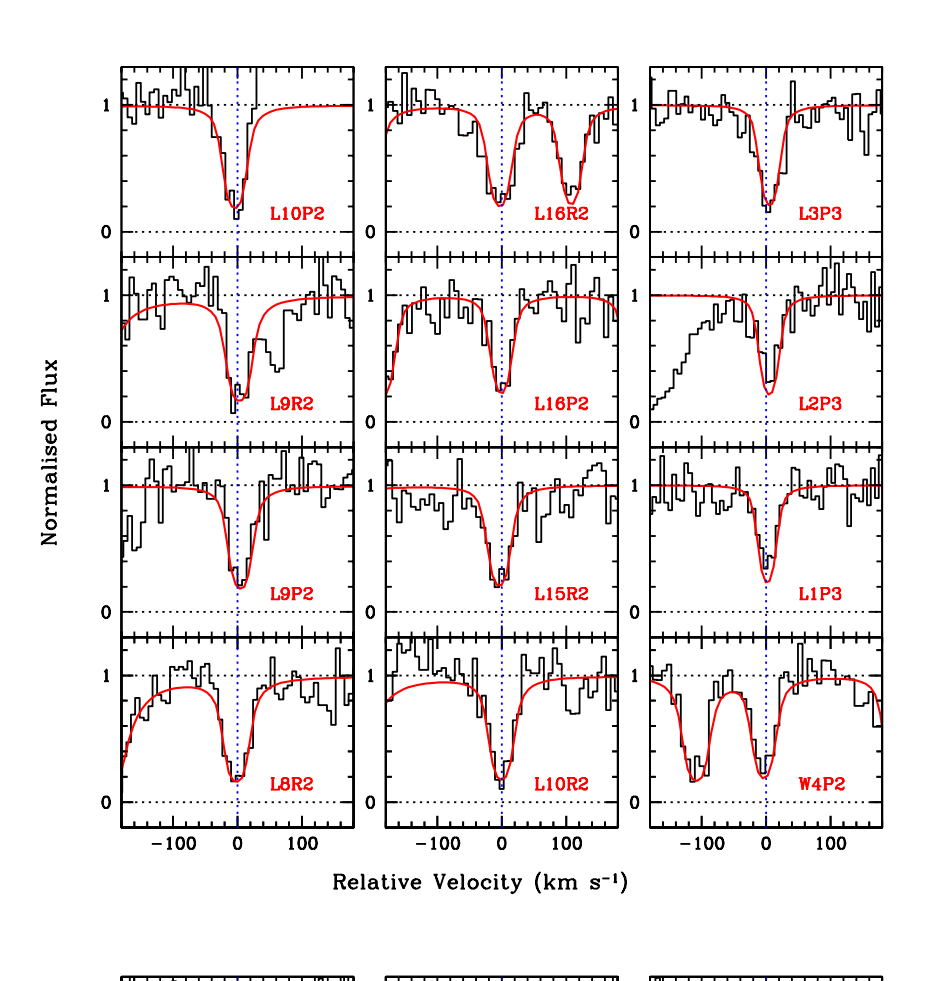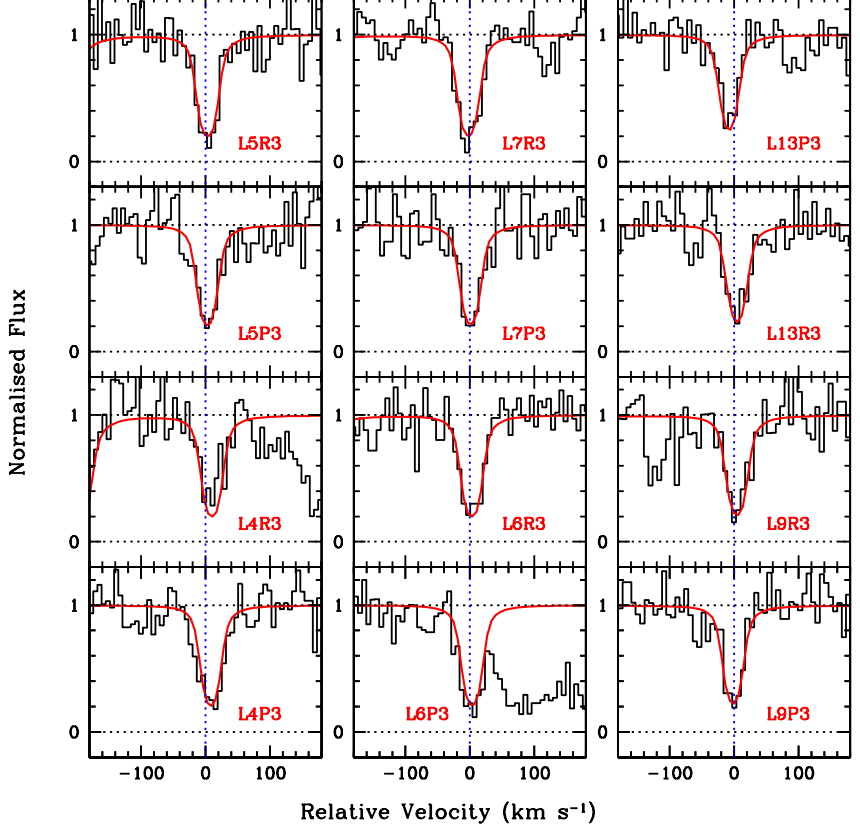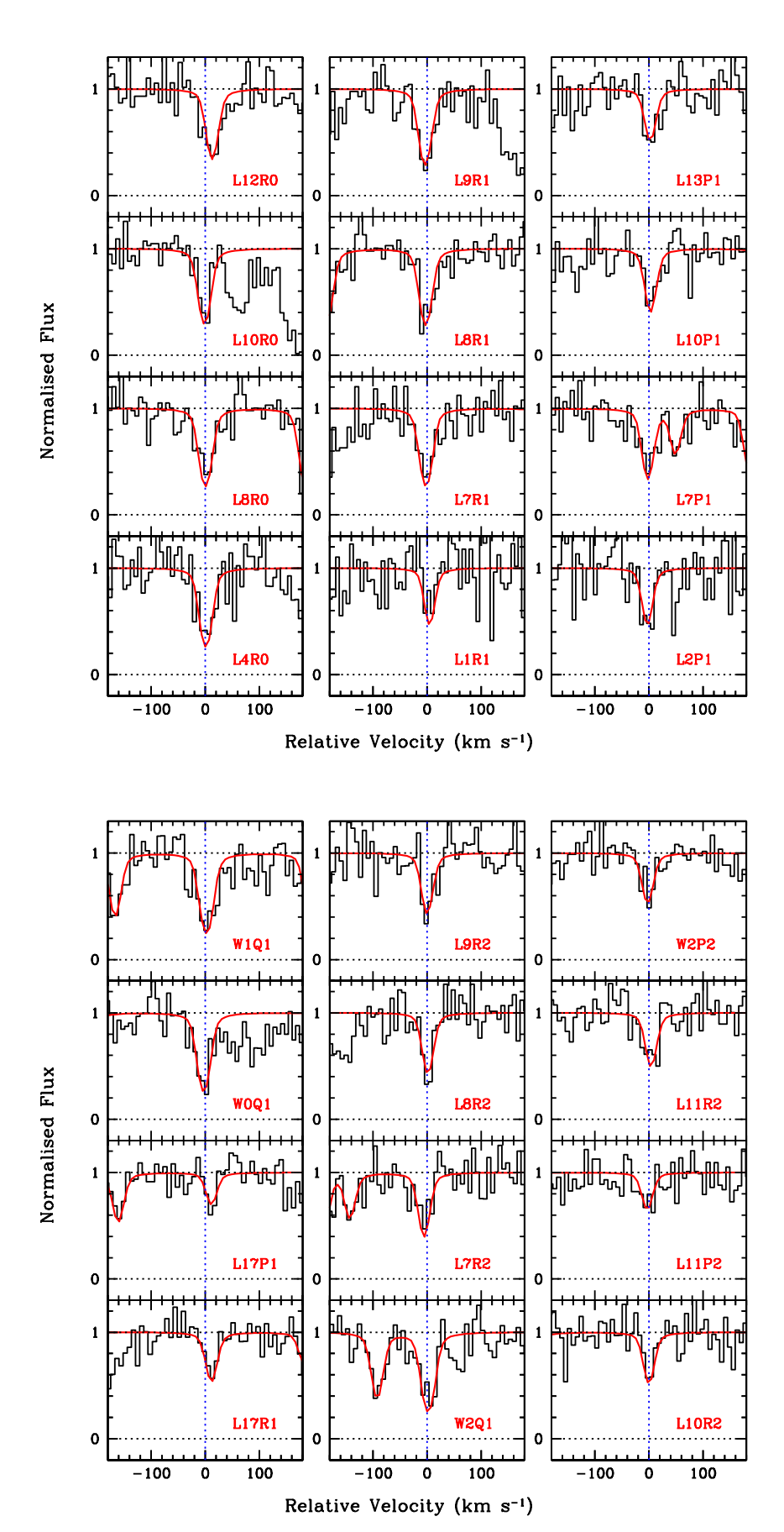
Figure C5. Continued.

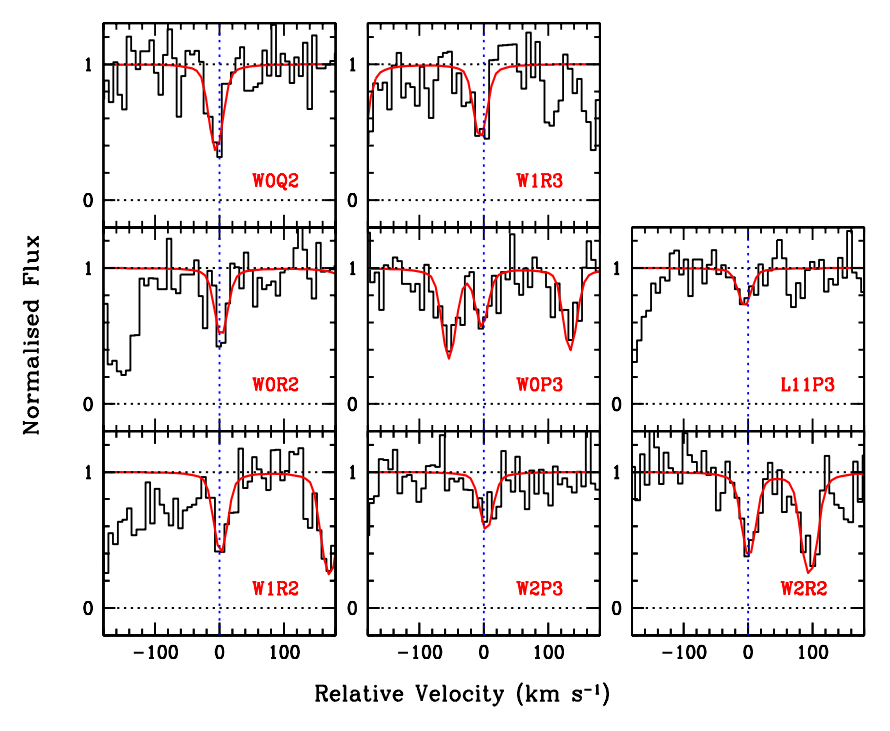**Figure C6.** Molecular hydrogen absorption from the $z_{\mathrm{abs}} = 0.55048$ towards Q1241+176 system.

Figure C6. Continued.